Structures of *Trypanosoma cruzi* Dihydroorotate Dehydrogenase Complexed with Substrates and Products: Atomic Resolution Insights into Mechanisms of Dihydroorotate Oxidation and Fumarate Reduction[†,‡]

Daniel Ken Inaoka,[§,||] Kimitoshi Sakamoto,[§] Hironari Shimizu,[§] Tomoo Shiba,[⊥] Genji Kurisu,[⊥] Takeshi Nara,[#] Takashi Aoki,[#] Kiyoshi Kita,[*,§] and Shigeharu Harada[*,○]

Department of Biomedical Chemistry, Graduate School of Medicine, The University of Tokyo, Tokyo 113-0033, Japan, Department of Life Sciences, Graduate School of Arts and Sciences, The University of Tokyo, Tokyo 153-8902, Japan, Department of Molecular and Cellular Parasitology, Juntendo University, Tokyo 113-8421, Japan, and Department of Applied Biology, Graduate School of Science and Technology, Kyoto Institute of Technology, Kyoto 606-8585, Japan

Received March 11, 2008; Revised Manuscript Received July 25, 2008

ABSTRACT: Dihydroorotate dehydrogenase (DHOD) from *Trypanosoma cruzi* (TcDHOD) is a member of family 1A DHOD that catalyzes the oxidation of dihydroorotate to orotate (first half-reaction) and then the reduction of fumarate to succinate (second half-reaction) in the *de novo* pyrimidine biosynthesis pathway. The oxidation of dihydroorotate is coupled with the reduction of FMN, and the reduced FMN converts fumarate to succinate in the second half-reaction. TcDHOD are known to be essential for survival and growth of *T. cruzi* and a validated drug target. The first-half reaction mechanism of the family 1A DHOD from *Lactococcus lactis* has been extensively investigated on the basis of kinetic isotope effects, mutagenesis and X-ray structures determined for ligand-free form and in complex with orotate, the product of the first half-reaction. In this report, we present crystal structures of TcDHOD in the ligand-free form and in complexes with an inhibitor, physiological substrates and products of the first and second half-reactions. These ligands bind to the same active site of TcDHOD, which is consistent with the one-site ping-pong Bi-Bi mechanism demonstrated by kinetic studies for family 1A DHODs. The binding of ligands to TcDHOD does not cause any significant structural changes to TcDHOD, and both reduced and oxidized FMN cofactors are in planar conformation, which indicates that the reduction of the FMN cofactor with dihydroorotate produces anionic reduced FMN. Therefore, they should be good models for the enzymatic reaction pathway of TcDHOD, although orotate and fumarate bind to TcDHOD with the oxidized FMN and dihydroorotate with the reduced FMN in the structures determined here. Cys130, which was identified as the active site base for family 1A DHOD (Fagan, R. L., Jensen, K. F., Bjornberg, O., and Palfey, B. A. (2007) *Biochemistry 46*, 4028–4036.), is well located for abstracting a proton from dihydroorotate C5 and transferring it to outside water molecules. The bound fumarate is in a twisted conformation, which induces partial charge separation represented as $C_2^{\delta-}$ and $C_3^{\delta+}$. Because of this partial charge separation, the thermodynamically favorable reduction of fumarate with reduced FMN seems to proceed in the way that $C_2^{\delta-}$ accepts a proton from Cys130 and $C_3^{\delta+}$ a hydride (or a hydride equivalent) from reduced FMN N_5 in TcDHOD.

Dihydroorotate dehydrogenase (DHOD[1]) is a flavoenzyme that catalyzes oxidation of (*S*)-dihydroorotate to orotate, the fourth step and the only redox reaction in the *de novo* pyrimidine biosynthesis pathway (Figure S1, Supporting Information). In the first half-reaction, oxidation of dihydroorotate is coupled with reduction of a flavin mononucleotide (FMN) cofactor. Based on amino acid sequence similarity, DHODs from different organisms can be divided into two families, family 1 and family 2 (*1*). Family 1 DHODs are cytoplasmic enzymes and can be further subdivided into families 1A and 1B. Family 1A enzymes

[†] This work was supported by grants to S.H. and K.K. from the Targeted Proteins Research Program (TPRP), Japan Aerospace Exploration Agency (JAXA), and in part by Grant-in-Aid for Scientific Research on Priority Areas, for the 21st Century COE Program and Creative Scientific Research from the Japanese Ministry of Education, Culture, Sports and Technology, and for Scientific Research (B) from Japan Society for the Promotion of Science. D.K.I. was a research fellow supported by Japan Society for the Promotion of Science.

[‡] Protein Data Bank coordinates and structure factors have been deposited as entries 2DJX for ligand-free TcDHOD, 2E6F for TcDHOD−oxonate, 2E68 for TcDHOD−dihydroorotate, 2E6A for TcDHOD−orotate, 2E6D for TcDHOD−fumarate and 2DJL for TcDHOD−succinate complexes.

* To whom correspondence should be addressed. K.K.: 7-3-1 Hongo, Bunkyo-ku, Tokyo 113-0033, Japan. Fax: (+81)-3-5841-3526. E-mail: kitak@m.u-tokyo.ac.jp. S.H.: Gosyokaidou-cho, Matsugasaki, Sakyo, Kyoto 606-8585, Japan. Fax: (+81)-75-724-7541. E-mail: harada@kit.ac.jp.

[§] Graduate School of Medicine, The University of Tokyo. Tel: +81-3-5841-3528.

[||] E-mail: danielken@m.u-tokyo.ac.jp.

[⊥] Graduate School of Arts and Sciences, The University of Tokyo.

[#] Juntendo University.

[○] Kyoto Institute of Technology. Tel: +81-75-724-7541.

[1] Abbreviations: DHOD, dihydroorotate dehydrogenase; FMN, flavin mononucleotide; FAD, flavin adenine dinucleotide; NAD, nicotinamide adenine dinucleotide; MWCO, molecular weight cutoff.

10.1021/bi800413r CCC: $40.75
Published on Web 09/23/2008

form homodimers and appear to utilize fumarate as a physiological oxidant, in conjunction with oxidation of the reduced FMN cofactor during the second half-reaction (*1*). In contrast, family 1B enzymes form heterotetramers and utilize NAD^+ via a distinct protein subunit that contains a 2Fe-2S cluster and FAD cofactor (*1*). Members of family 2 exist as homodimers or monomers and are membrane-bound enzymes that utilize respiratory quinone as a physiological oxidant during the second half-reaction (*2*−*4*). The N-terminal domain found only in family 2 DHODs forms the binding site for quinone (*5*).

Many inhibitors targeting the quinone binding-site have been designed such as human DHOD inhibitor leflunomide that is in clinical use to treat rheumatoid arthritis (*5*). Other potent and selective inhibitors designed for family 2 DHODs from *Escherichia coli* (*6*), *Helicobacter pylori* (*7*) and *Plasmodium falciparum* (*2, 8, 9*) inhibit their growth. These inhibitors designed for family 2 DHODs are not effective against family 1A DHODs, since family 1A lacks the quinone binding site. On the other hand, hydroxybenzoates such as 3,4-dihydroxybenzoate and 3,5-dihydroxybenzoate are inhibitors specific for family 1A DHODs (*10, 11*), although these inhibitors with IC_{50}s in the range of micromolar order are not potent. Previously, we reported the organization and amino acid sequences of all enzymes in the *de novo* pyrimidine biosynthesis pathway of *Trypanosoma cruzi* (*12*). In that work, we found that the *T. cruzi pyr4* gene product is homologous to family 1A DHODs from *Lactococcus lactis* and *Saccharomyces cerevisiae*. DHOD from *T. cruzi* (TcDHOD) is 313 amino acids in length (Figure 1) and exists in cells as a homodimer (MW 2 × 34 kDa). In addition to DHOD activity, TcDHOD also shows fumarate reductase activity, suggesting that it is involved not only in the *de novo* pyrimidine biosynthesis pathway but also in redox homeostasis of the parasite (*12*−*14*). Recently, Annoura et al. (*15*) demonstrated that TcDHOD knockout *T. cruzi* could not survive even in the presence of substrates for enzymes of pyrimidine salvage pathway. The importance of DHOD to survival of *Trypanosoma brucei* in the blood stream form was also shown by Arakaki et al. (*16*). Therefore, the enzyme has the characteristics of a promising target for the development of chemotherapeutic agents to combat infections with the pathogen.

To date, X-ray structure analyses have been performed for seven DHODs from six organisms: family 1A DHODs from *L. lactis* (*17*) and *T. brucei* (*16*), family 1B DHOD from *L. lactis* (*18*), and family 2 DHODs from *E. coli* (*4*), *P. falciparum* (*19*), *Rattus rattus* (*20*) and *Homo sapiens* (*5*). Although kinetic studies of the catalytic mechanism for DHOD have extensively been performed (*21*−*30*), none of the structures determined to date include DHOD in a complex with a physiological substrate. In this study, we determined the crystal structures of TcDHOD in the ligand-free form, in complexes with substrates and products of the first and second half-reactions, and in a complex with an inhibitor, oxonate at atomic resolution. These structures, in particular those of TcDHOD complexed with dihydroorotate and fumarate, provided us further insights into the catalytic mechanisms of dihydroorotate oxidation and fumarate reduction.

EXPERIMENTAL PROCEDURES

Cloning, Expression and Purification. Recombinant TcDHOD was expressed, purified and crystallized as previously reported (*31*). Briefly, TcDHOD was purified to homogeneity using DEAE Fast Flow (GE Healthcare) followed by Phenyl Sepharose H.P. (GE Healthcare) and TSK G3000SW (Tosoh). A total of 11 mg of TcDHOD with high specific activity (12.5 μmol/min/mg) was purified from 10 L of culture (Table S1, Supporting Information). The addition of 0.25 mM orotate during purification and storage was indispensable to stabilize the enzymatic activity.

Protein Assay and FMN Content Determination. Protein concentrations were determined according Lowry with bovine serum albumin as the standard (*32*). The FMN content of the purified TcDHOD was estimated to be 1.0 using a spectroscopic method, on the basis of the extinction coefficient of FMN (11.1 mM^{-1} cm^{-1} at 450 nm).

Enzyme Assay. DHOD activity was measured as described previously (*14*) with minor modifications. Orotate production was assayed by measuring the absorption at 290 nm (ε = 6.4 × mM^{-1} × cm^{-1}). The reaction was started by adding 0.5 mM dihydroorotate into the reaction mixture containing 50 mM potassium phosphate buffer pH 7.5, 2 mM sodium fumarate and TcDHOD in a final volume of 1 mL.

Crystallization. The plate-shaped dark-orange crystals of the TcDHOD−orotate complex with the oxidized FMN cofactor were obtained at 277 K by the hanging drop vapor diffusion method using 16% (w/v) PEG 3350, 100 mM sodium cacodylate pH 6.2, 1 mM sodium orotate, 50 mM hexaamminecobalt (III) chloride and 1 mM sodium thiocyanate as the reservoir solution (*31*). The TcDHOD−oxonate complex was prepared by repeated concentration and dilution of the purified enzyme with a buffer containing oxonate using an Amicon Ultra-4 10,000 MWCO filter. This was followed by cocrystallization in a similar manner as described above except that cocrystallization was carried out in the presence of 1 mM oxonate instead of orotate at pH 5.1. Crystals of the ligand-free TcDHOD were prepared by back-soaking crystals of the TcDHOD−oxonate complex in buffer A (100 mM cacodylate pH 5.1, 20% (w/v) polyethylene glycol 3350, 50 mM hexaamminecobalt (III) chloride and 1 mM sodium thiocyanate) for three days with repeated buffer exchange. Crystals of the TcDHOD−succinate and −fumarate complexes were prepared by soaking ligand-free crystals for three days in buffer A containing 10 mM succinate or fumarate, respectively. Crystals of the TcDHOD−dihydroorotate complex were obtained by soaking ligand-free crystals for 10 to 15 s in buffer A containing 10 mM dihydroorotate plus 15% (w/v) glycerol. During soaking, the color of the crystals changed from dark to light orange, which indicates that the FMN cofactor was reduced by dihydroorotate. After soaking, a crystal mounted in a nylon loop was immediately flash-frozen in a nitrogen stream at 100 K, and X-ray diffraction data were collected. During data collection, the light orange color of the crystals was kept. Since kinetic analysis indicated that dihydroorotate can be bound to TcDHOD with the reduced FMN cofactor if an excess amount of dihydroorotate is present (*14, 26*), the crystals prepared should be those of the TcDHOD−dihydroorotate complex with the reduced FMN cofactor.

FIGURE 1: Multiple alignment of amino acid sequences of DHODs. The alignment was produced from fourteen amino acid sequences from family 1A (*T. cruzi*/AB212956.1, *T. brucei*/AC159455.1, *L. lactis*/X74206.1, *Streptococcus pneumoniae*/ABJ54983.1 and *Saccharomyces kluyveri*/AY323902.1), catalytic subunit of family 1B (*L. lactis*/CAA52280.1, *Streptococcus thermophilus*/AAV62538.1, *Enterococcus faecalis*/AAO81490, *Clostridium tetani*/AAO36852.1 and *Clostridium cellulolyticum*/ZP_01576243.1) and family 2 (*E. coli*/CAA26594.1, *P. falciparum*/CAG25203.1, *R. rattus*/CAA56765.1 and *H. sapiens*/AAA50163.1) DHODs using CLUSTAL-W. Alignment of eight DHODs, whose structures are known, is shown. They belong to family 1A (*T. cruzi*, *T. brucei* and *L. lactis* A), family 1B (*L. lactis* B) or family 2 (*E. coli*, *P. falciparum*, *R. rattus* and *H. sapiens*). Their PDB codes are 2DJX (this study), 2B4G (*16*), 2DOR (*29*), 1EP2 (*18*), 1F76 (*4*), 1TV5 (*19*), 1UUO (*20*) and 1D3G (*5*), respectively. In yellow, residues conserved in more than one family. In red, those conserved only within a family. Secondary structural elements of the TcDHOD structure are also indicated; β strands are shown as arrows and α helices as squiggles. Residues involved in interactions with FMN, oxonate, dihydroorotate, orotate, fumarate or succinate are marked with an asterisk. TcDHOD Lys43, Glu125, Cys130 and Lys164, which are mentioned in Discussion, along with their structurally equivalent residues in other DHODs, are colored blue. The numbers shown for amino acid residues of the TcDHOD protein referred to those of *L. lactis* DHODA.

X-ray Data Collection, Phasing and Refinement. X-ray diffraction data sets for TcDHOD in the ligand-free form and in complexes with orotate, fumarate and succinate were collected at 100 K with beamline BL44XU from SPring-8 (λ = 0.900 Å) in Harima, Japan, using a Bruker AXS DIP6040 detector. Data sets for TcDHOD−oxonate and −dihydroorotate complexes were collected at 100 K with beamline NW12 of Photon Factory Advanced Ring (λ = 1.000 Å) in Tsukuba, Japan, using an ADSC Quantum-210 detector. All data sets were indexed, integrated and scaled using *HKL2000* (*33*). Table 1 summarizes data collection statistics. The structure of the TcDHOD−orotate complex was solved by the molecular replacement method using *Molrep* (*34*). A search model was generated from a single monomer of the *L. lactis* DHODA dimer structure (PDB code, 2DOR; 55% sequence identity with TcDHOD) with all non-protein atoms removed. The sequence was changed to that of TcDHOD by applying the TcDHOD sequence (NCBI accession number BAE48283 (*35*)) onto the search model using Swiss-Pdb Viewer (*36*). The molecular replace-

Table 1: Data Collection and Refinement Statistics[a]

	ligand-free	oxonate	dihydroorotate	orotate	fumarate	succinate
			Data Collection			
space group	$P2_12_12_1$	$P2_12_12_1$	$P2_12_12_1$	$P2_12_12_1$	$P2_12_12_1$	$P2_12_12_1$
cell dimensions						
a, *b*, *c* (Å)	69.96, 73.13, 126.09	68.36, 71.83, 123.64	68.44, 71.94, 123.85	68.25, 71.88, 123.57	68.28, 71.88, 123.61	68.15, 71.77, 123.40
wavelength (Å)	0.9	1.0	1.0	0.9	0.9	0.9
resolution (Å)	50.0−1.58 (1.64−1.58)	50.0−1.26 (1.29−1.26)	50.0−1.38 (1.43−1.38)	50.0−1.64 (1.70−1.64)	50.0−1.94 (2.01−1.94)	50.0−1.38 (1.43−1.38)
R_{merge} (%)	7.0 (39.8)	7.1 (39.5)	8.4 (39.6)	7.8 (39.8)	9.9 (24.4)	6.0 (33.0)
$I/\sigma(I)$	8.2 (2.76)	8.5 (3.04)	10.5 (4.26)	9.9 (3.12)	12.8 (8.19)	9.0 (2.62)
completeness (%)	98.5 (99.4)	97.7 (99.2)	97.5 (98.9)	96.1 (97.9)	99.9 (100.0)	94.9 (69.5)
redundancy	4.0	4.4	4.6	3.7	6.1	5.2
			Refinement			
resolution (Å)	40.0−1.58	30.0−1.26	30.0−1.38	50.0−1.64	50.0−1.94	50.0−1.38
no. of reflections	86263	152389	116503	68521	43381	112910
R-factor/*R*-free	0.182/0.204	0.166/0.180	0.169/0.183	0.164/0.192	0.158/0.200	0.166/0.183
no. of atoms						
protein	4758	4758	4758	4758	4758	4758
FMN	31	31	31	31	31	31
ligand	0	22	22	22	16	16
water	689	799	637	497	476	696
B-factors						
protein	17.1	9.9	12.0	10.7	9.7	12.0
FMN	11.5	5.7	4.5	6.1	5.1	7.4
ligand		6.8	7.4	5.6	11.8	9.6
water	25.0	19.6	18.0	20.9	17.5	21.2
rms deviations						
bond lengths (Å)	0.009	0.007	0.008	0.011	0.015	0.007
bond angles (deg)	1.219	1.171	1.219	1.309	1.438	1.192

[a] Highest-resolution shell is shown in parentheses.

ment was carried out under different resolution ranges of 2.0−8.0, 3.0−8.0 and 4.0−8.0 Å. Essentially consistent solutions giving one TcDHOD dimer in the asymmetric unit were obtained. The resulting model obtained after rigid-body refinement was refined at 2.5 Å resolution under strict noncrystallographic symmetry (NCS) restraints using *CNS* (*37*), and electron-density maps calculated with σ_A-weighted $2F_o - F_c$ and $F_o - F_c$ coefficients were generated and inspected to check the validity of the initial model. After a few rounds of refinement and manual rebuilding using *CNS* and *Coot* (*38*), respectively, FMN cofactors and orotate molecules became clearly visible on electron-density maps and were incorporated into the model. Subsequently, the model was subjected to iterative cycles of refinement and manual rebuilding at 1.64 Å resolution using isotropic temperature factors and weak NCS restraints. At this stage, many water molecules were identified using electron-density maps (3σ cutoff). The model was finally refined using *Refmac5* (*39*) and *Coot* without NCS restraints, resulting in *R*-factor and *R*-free values of 0.164 and 0.192, respectively. In the final homodimer model of the TcDHOD−orotate complex, each subunit consists of 312 amino acid residues from Met0 to Ile311, one oxidized FMN cofactor and one orotate molecule. The C-terminal amino acid residue, Glu312, could not be defined on the final $2F_o - F_c$ electron density map. In the Ramachandran plot (*40*), 93.2% of the residues are in the most favored regions and 6.8% are in additionally allowed regions, as defined by *PROCHECK* (*41*). The structures of the ligand-free TcDHOD and the complexes with dihydroorotate, oxonate, fumarate and succinate were refined starting from the protein atom coordinates of the TcDHOD−orotate complex. Coordinate files and appropriate restrains for those ligands were generated using the PRODRG server and Sketcher program of the CCP4 suite (*42*).

Successful preparations of crystals of the ligand-free TcDHOD and those of TcDHOD in complexes with dihydroorotate, fumarate and succinate were confirmed by inspecting $2F_o - F_c$ electron density maps calculated after omit refinement (Figure S2 A−L, Supporting Information). In the map calculated for the ligand-free TcDHOD (Figure S2 A, B), four water molecules located near the FMN isoalloxazine ring in the active site were assigned. Well-shaped electron dense regions corresponding to dihydroorotate, fumarate or succinate were also recognized in the active site of each complex. Refinement statistics for all models are summarized in Table 1.

RESULTS

Overall Structure. In the presence of orotate, the TcDHOD protein, consisting of 313 amino acid residues and one oxidized FMN cofactor, was crystallized in orthorhombic space group $P2_12_12_1$ with two identical subunits related by a noncrystallographic 2-fold axis present in the crystallographic asymmetric unit. Crystals of the ligand-free TcDHOD and of TcDHOD in complexes with the substrates (dihydroorotate and fumarate), products (orotate and succinate) and the inhibitor (oxonate) were prepared as described in Experimental Procedures. Crystals of TcDHOD−dihydroorotate complex included the reduced FMN cofactor, but the other five crystal forms included the oxidized FMN cofactor. All structures determined included a 312 amino acid region from Met0 to Ile311 of the full-length protein but the C-terminal Glu312 was not assigned. Figure 1 shows a multiple amino acid sequence alignment of TcDHOD and

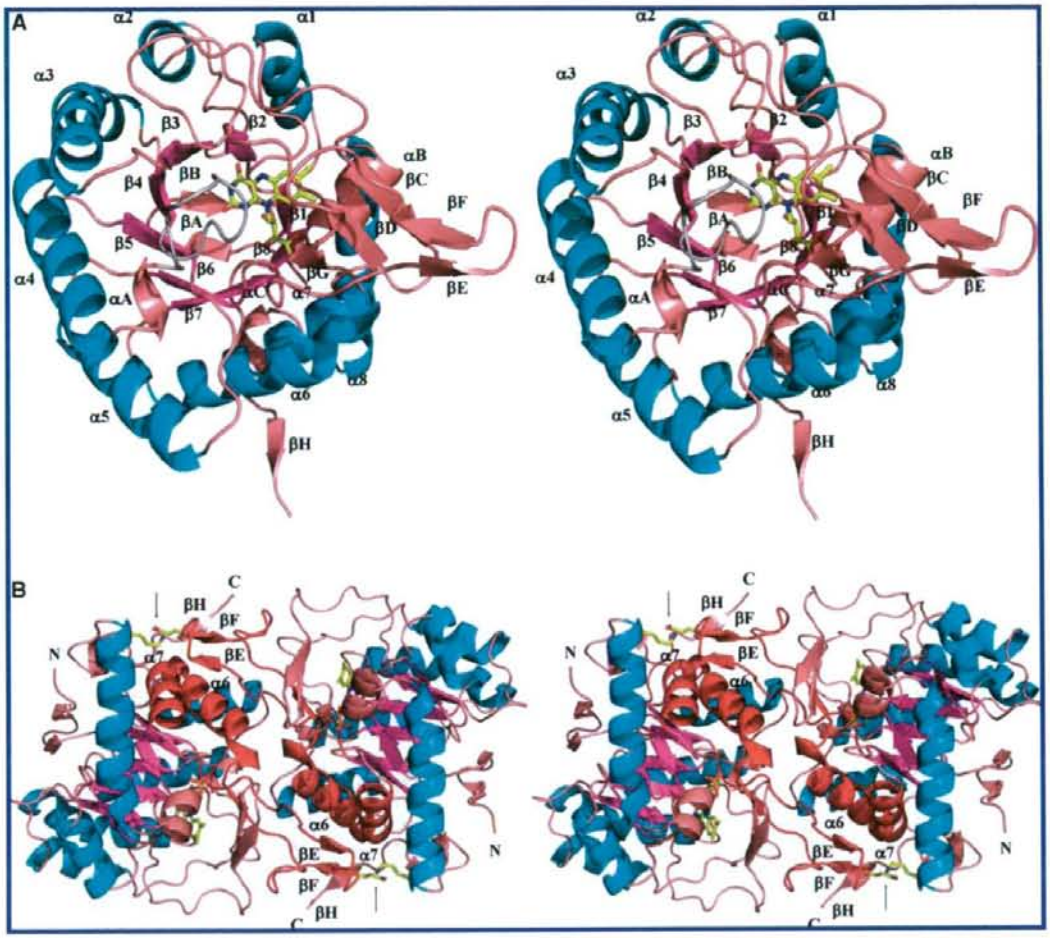

FIGURE 2: Structure of ligand-free TcDHOD (stereo views). (A) Ribbon diagram of the TcDHOD subunit structure. The $(\alpha/\beta)_8$ barrel is represented in blue (α-helices) and magenta (β-strands); the β4−αA loop, the active site loop, is shown in gray; and the FMN cofactor is shown in yellow. The color code for each atom type is as follows: red, oxygen; blue, nitrogen; orange, phosphate. The same color-code was applied to all figures. (B) The dimer structure viewed from above the 2-fold axis. The $(\alpha/\beta)_8$ barrel of each subunit is color-coded as described in (A). The β6−α6 loops, helices α6 and α7, which participate in dimer interface interactions, are in red. Arrows indicate intersubunit salt bridges between Glu207 and Lys296, shown in yellow. The images were generated using PyMOL (http://pymol.sourceforge.net).

seven DHODs with known structures. Figures 2A and 2B show the subunit and homodimer structures of the ligand-free TcDHOD. As there are no significant differences between the structures of the two subunits, as indicated by a root-mean-square (rms) deviation of 0.20 Å calculated for superimposed 312 C_α positions, we will instead focus on one subunit to describe the structure as a whole.

The overall structure of TcDHOD is very similar to those of other DHODs listed in Figure 1. The C_α atoms of a TcDHOD subunit can be superimposed on the structurally equivalent 311 C_α atoms of *T. brucei* DHOD (PDB code, 2B4G) or the 298 C_α atoms of *L. lactis* DHODA (2DOR) with rms deviations of 0.39 and 0.82 Å, respectively, which indicates that the main-chain structures of these three DHODs, especially TcDHOD and *T. brucei* DHOD, are essentially identical. The rms deviations for DHODs from different families are somewhat larger; namely, for the family 1B member *L. lactis* DHODB (1EP2), rms deviation of 1.94 Å for 270 C_α atoms and for family 2 members, as follows, 1.76 Å for 253 C_α atoms of *E. coli* DHOD (1F76), 1.68 Å for 275 C_α atoms of *P. falciparum* DHOD (1TV5), 1.81 Å for 186 C_α atoms of *R. rattus* DHOD (1UUO) and 1.74 Å for 272 C_α atoms of *H. sapiens* DHOD (1D3G). In addition, the dimer structure of DHOD from *T. cruzi* Y strain, in which TcDHOD Phe61 is replaced by a valine residue, was determined at 2.2 Å resolution as a form with a sulfate ion bound to its active site ((*43*); PDB code 3C3N), during the submission of this article. TcDHOD is very similar to 3C3N as indicated by the rms deviation of 0.44 Å.

As is true for the many other flavin containing proteins, TcDHOD subunits fold into an $(\alpha/\beta)_8$ motif with a parallel eight-stranded β-barrel (β1−β8) surrounded by eight α-helices (α1−α8), with the FMN cofactor on the C-terminal end of the β-barrel. Each of the secondary structural elements of the $(\alpha/\beta)_8$ motif is connected to the next one via a short loop consisting of several amino acid residues. The loops

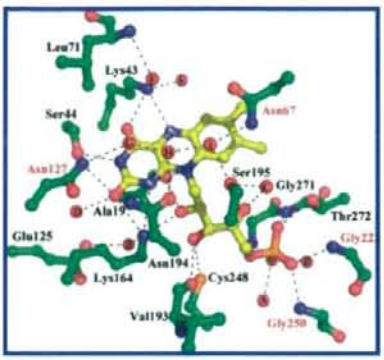

FIGURE 3: The environment of the FMN cofactor of the ligand-free TcDHOD. Amino acid residues and the FMN cofactor are indicated by green or yellow ball-and-stick models, respectively, and ten water molecules (A−J) that were assigned in this region are also shown. Hydrogen bonds are represented by dotted lines. Residue names shown by red are conserved in the amino acid sequences of all known DHODs. The images were generated using PyMOL (http://pymol.sourceforge.net).

connecting β2 and α2 (β2−α2 loop, residues 43−75), β4 and α4 (β4−α4 loop, residues 128−142) and β6 and α6 (β6−α6 loop, residues 193−222) are longer than the others and include additional secondary structural elements. Moreover, in each subunit, βC, βD in the β2−α2 loop and βG in the β6−α6 loop form a three-stranded antiparallel β-sheet, whereas βE and βF in the β6−α6 loop form a two-stranded antiparallel β-sheet (Figure 2A). In the dimer structure, the β6−α6 loop protrudes from one subunit toward α6 and α7 of the other, forming dimer interfaces. Each interface includes an intersubunit three-stranded β-sheet composed of βE and βF of one subunit plus βH of the other, and an intersubunit salt bridge between Glu207 and Lys296 (Figure 2B). Additionally, hydrophobic interactions occur between subunits.

The FMN cofactor is well buried except for a partially exposed dimethyl benzene moiety. One side of the FMN isoalloxazine ring faces toward the C-terminal end of the barrel, and the other side is veiled in three long β2−α2, β4−αA (residues 128−138) and β6−α6 loops. In particular, the β4−αA loop, which includes an amino acid sequence that is highly conserved among all DHODs (Figure 1) and has been identified as the active site loop in *L. lactis* DHODA (*22*, *28*) and *E. coli* DHOD (*44*), is located just over the FMN cofactor, preventing an outside solvent from contacting the isoalloxazine ring (Figure 2A). Figure 3 shows amino acid residues and bound water molecules in the FMN cofactor region. Nitrogen and oxygen atoms of the isoalloxazine ring interact via hydrogen bonds with Ala19 O, Lys43 N_ζ, Ser44 O, Asn127 $N_{\delta2}$, Lys164 N_ζ and water D, but the hydrophobic dimethyl benzene moiety lacks close contacts with amino acid residues of TcDHOD. In addition, ribityl hydroxyl groups interact with Ala19 O, Lys164 N_ζ, Val193 O, Cys248 S_γ and water C, and the phosphate group interacts with main chain imino nitrogen atoms of Gly222, Gly250, Gly271 and Thr272 as well as Thr272 $O_{\gamma1}$, water A and B. Three hydrogen bonds formed between Lys164 and the isoalloxazine should play a crucial role in binding FMN to TcDHOD, as indicated by the K164A mutant of *L. lactis* DHODA, to which FMN does not bind (*22*). The negative charge on the phosphate group seems to be stabilized by hydrogen bonds with these main chain imino nitrogen atoms, as has been observed for the oxyanion holes of serine proteases (*45*). There are four water molecules (F, G, H and I) in each cavity formed between the isoalloxazine ring and the β4−αA loop. These water molecules interact with one another and with Asn67 $N_{\delta2}$, Leu71 N, Asn127 $N_{\delta2}$, Asn194 $O_{\delta1}$ and Ser195 O_γ. Most of the amino acid residues referred to here have been completely or well conserved in all known DHOD sequences and participate in interactions with FMN cofactors in the structures of DHODs listed in Figure 1.

Binding of Dihydroorotate, Orotate and Oxonate to TcDHOD. (*S*)-Dihydroorotate, orotate and oxonate are a substrate, product and competitive inhibitor of DHODs, respectively (*21*). Figures 4A−C show that each of these compounds binds to the cavity in the same manner, at the position occupied by waters F, G, H and I in the ligand-free structure. Correspondingly, O8, O4, N3 and O2 of each compound are positionally related to waters F, G, H and I, respectively. In the bound form, orotate and oxonate are in a planar conformation with the exception of their carboxyl oxygen atoms. For dihydroorotate, by contrast, C5 and C6 deviate from the plane constituted by N1, C2, N3, C4, O2 and O4 at a distance and direction of 0.20 Å away from or 0.29 Å toward the isoalloxazine ring, respectively. The dihydroorotate carboxyl group is in an equatorial conformation and faces away from the isoalloxazine ring, whereas the calculated position of the axial C6 hydrogen, H6, is located between C6 and FMN N5 (Figure 4A).

The bound dihydroorotate, orotate and oxonate stack parallel to the isoalloxazine ring and do not appear to cause any discernible changes in the conformation of the TcDHOD polypeptide as compared with the ligand-free form. These compounds interact via hydrogen bonds with Lys43 N_ζ, Asn67 $O_{\delta1}$ and $N_{\delta2}$, Gly70 N, Asn127 $N_{\delta2}$, Asn132 $N_{\delta2}$, Asn194 $O_{\delta1}$ and $N_{\delta2}$, Met69 N, Leu71 N and Ser195 O_γ. The carboxyl groups of dihydroorotate, orotate and oxonate are twisted about their C_6-C_7 bonds with $C_5-C_6-C_7-O_9$ dihedral angles of 98.5°, 127.0° and 113.2°, respectively. Their carboxyl O_8 atoms interact with Lys43 N_ζ and Leu71 N, and their carboxyl O_9 atoms with Gly70 N, Met69 N and Asn132 $N_{\delta2}$ (Figures 4A−C). Interactions that involve protein nitrogen atoms are commonly found in the structures of other DHOD−orotate complexes, and seem to be involved in stabilization of negative charges on their carboxyl groups and of the twisted conformation.

Cys130 in the β4-αA loop, which has previously been identified as the catalytic base in *L. lactis* DHODA (*21*−*23*, *28*, *29*), is located with its S_γ at distances of 3.52 Å, 4.94 Å and 4.46 Å from dihydroorotate C_5, O_8 and O_9, respectively. Nearly equal distances were also determined for the distance between S_γ and orotate C_5, O_8 and O_9 (that is, 3.62 Å, 4.92 Å and 4.66 Å, respectively). In both cases, the distance from S_γ to O_8 or O_9 is too far for the thiol group to interact with either, according to the van der Waals radii for SH (2.34 Å) and O (1.40 Å) (*46*). However, the distances between S_γ and C_5 are favorable for a $S_\gamma\cdots H-C_5$ interaction in the bound dihydroorotate, and for a $S_\gamma-H\cdots C_5$ interaction in the bound orotate (Figures 4A,B).

Oxonate, a competitive inhibitor for all DHODs (*21*) (IC_{50} = 35 μM for TcDHOD), appears to be bound to TcDHOD in the same manner observed for dihydroorotate and orotate

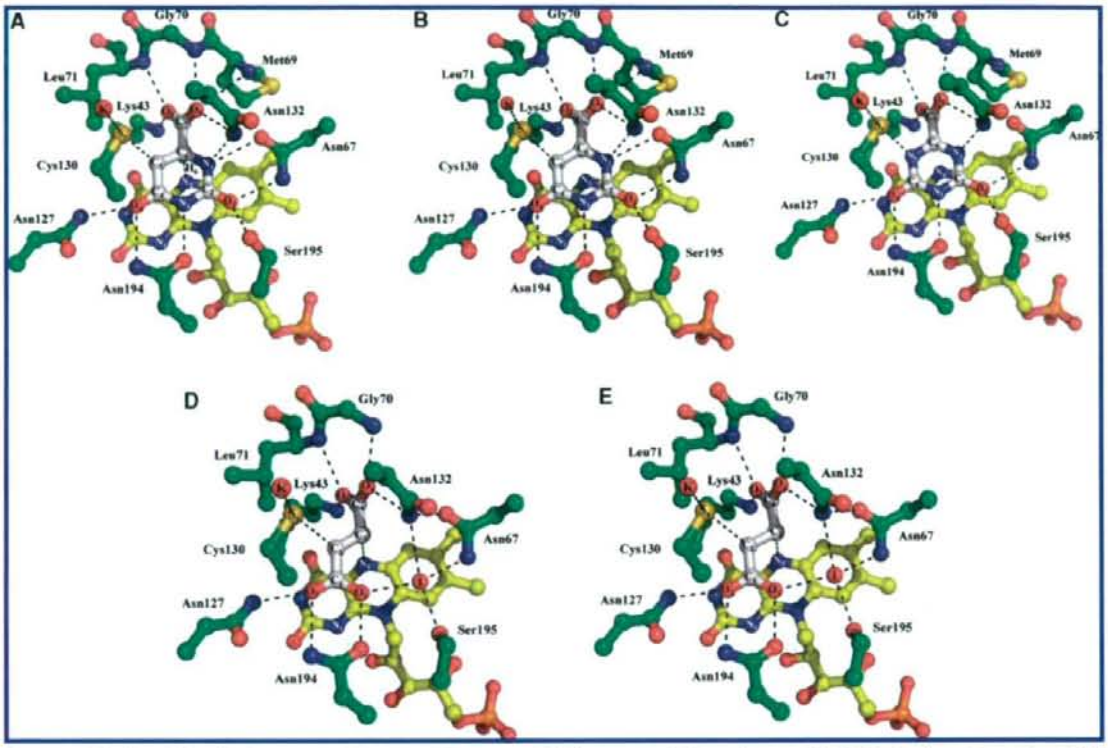

FIGURE 4: Binding of (A) dihydroorotate, (B) orotate, (C) oxonate, (D) fumarate and (E) succinate to TcDHOD. Amino acid residues, FMN and bound compounds are shown as green, yellow or white ball-and-stick models, respectively. The substrates and products of the first half-reaction (dihydroorotate and orotate) and second half-reaction (fumarate and succinate) and a competitive inhibitor (oxonate) are bound to TcDHOD in a similar manner. In (A)−(E), Cys130 Sγ forms a hydrogen bond with water K and is located 3.52 Å, 3.62 Å, 3.42 Å, 3.43 Å and 3.60 Å from dihydroorotate C_5, orotate C_5, oxonate N_5, fumarate C_2 and succinate C_2, respectively. The FMN N_5 is located 3.25 Å, 3.65 Å, 3.66 Å, 3.51 Å and 3.32 Å from dihydroorotate C_6, orotate C_6, oxonate C_6, fumarate C_3 and succinate C_3, respectively. In each structure, possible hydrogen bond interactions are shown only for those between the compounds and TcDHOD, and are represented by dotted lines. The images were generated with PyMOL (http://pymol.sourceforge.net).

(Figure 4C). The distances between oxonate O_9 and Met69 N, oxonate N_1 and Asn67 $O_{\delta 2}$ are longer by 0.28−0.46 Å than those observed in the bound dihydroorotate and orotate. However, an additional hydrogen bond with a distance of 3.41 Å is formed between oxonate N_5 and Cys130 S_γ. This interaction probably contributes to a decrease in the average *B*-factor of the main-chain atoms of the β4−αA loop to 6.9 Å^2 as compared with 9.4 Å^2 and 15.0 Å^2 for the TcDHOD−dihydroorotate and −orotate complexes, respectively, and thus, to suppression of the flexibility of the β4−αA loop.

Binding of Fumarate and Succinate to TcDHOD. Both fumarate and succinate are bound to the same site as dihydroorotate, orotate and oxonate via identical hydrogen bonds with TcDHOD amino acid residues (Figures 4D,E). The bound fumarate and succinate are in a planar conformation, approximately parallel to the isoalloxazine ring, with the exception of the second carboxyl O_3 and O_4 atoms. As observed in the bound dihydroorotate, orotate and oxonate, the second carboxyl groups are twisted about the C3−C4 bonds with $C_2-C_3-C_4-O_4$ dihedral angles of 99.1° and 92.4°, respectively, and interact with protein nitrogen atoms. On the other hand, the first carboxyl C_1, O_1 and O_2 atoms occupy the C_4, O_4 and N_3 positions, respectively, of the bound dihydroorotate *etc.*

C_2 and C_3 of the bound fumarate and succinate are in close contact with Cys130 S_γ and FMN N_5, respectively. The distances between S_γ and C_2 are 3.43 and 3.60 Å for the bound fumarate and succinate, respectively, and those between N_5 and C_3, 3.51 and 3.32 Å. Accordingly, S_γ and C_2, as observed in the bound dihydroorotate *etc.*, are also at a distance favorable for a $S_\gamma-H\cdots C_2$ interaction in the bound fumarate, and for a $S_\gamma\cdots H-C_2$ interaction in the bound succinate (Figures 4D,E).

DISCUSSION

In this study, we determined, at atomic resolution, the structures of TcDHOD in the ligand-free form and in complexes with physiological substrates (dihydroorotate and fumarate) and reaction products (orotate and succinate), as well as in a complex with the competitive inhibitor oxonate. We found that the substrates and products of the first and the second half-reactions bind to the same site of TcDHOD, which is consistent with the one-site ping-pong Bi-Bi mechanism demonstrated by kinetic studies for family 1A DHODs (*14, 26, 27, 47*). The structures of each of the five complexes can be superimposed on the ligand-free structure with an rms deviation in the range 0.11 Å to 0.13 Å for subunit 312 C_α positions, and 0.12 Å to 0.16 Å for dimer

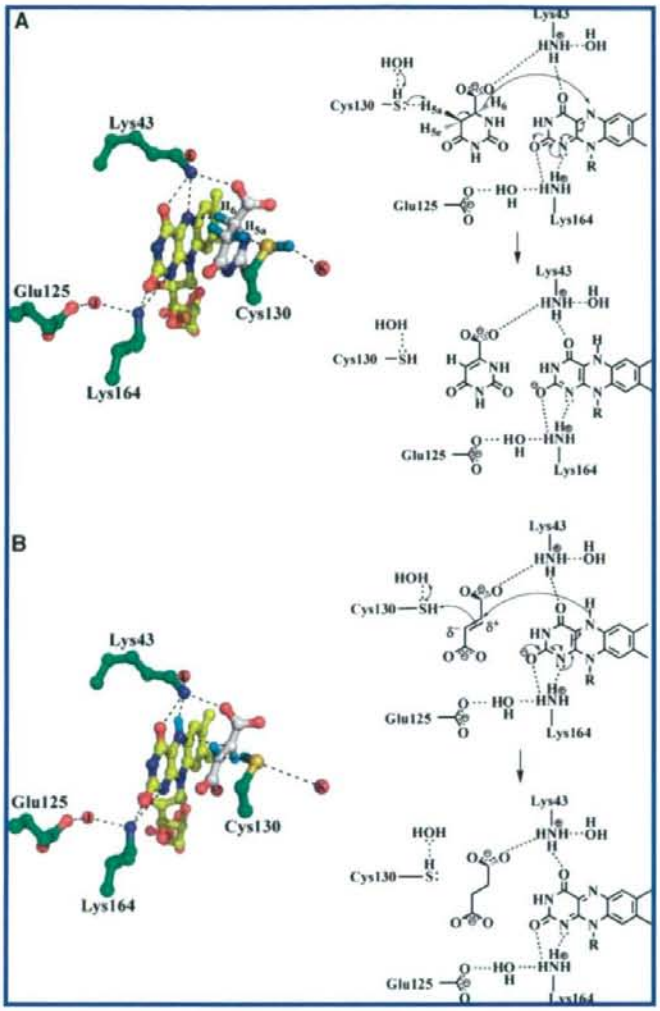

FIGURE 5: Proposed mechanisms for (A) the first half-reaction (oxidation of dihydroorotate to orotate) and (B) the second half-reaction (reduction of fumarate to succinate) as carried out by TcDHOD. The FMN cofactor (yellow), amino acid residues (green) and substrates (white) are represented using ball-and-stick models drawn with PyMOL. The hydrogen atoms of dihydroorotate C5, C6 and Cys130Sγ are shown at their calculated positions (cyan balls).

624 C_α positions. Furthermore, in each structure we determined, both the oxidized and the reduced FMN cofactors are essentially planar, and the FMN cofactor and its peripheral 72 amino acid residues within 8 Å can be superimposed on the ligand-free form, with an rms deviation of 0.06 Å to 0.10 Å between subunits, and 0.08 Å to 0.11 Å between dimers. Thus, the protein and FMN cofactor portions of the complexes are essentially identical with the ligand-free TcDHOD. Although structures determined in this study do not reveal physiological states in the sense that orotate and fumarate bind to TcDHOD with the oxidized FMN cofactor and dihydroorotate binds to TcDHOD with reduced FMN, they should be good models for the TcDHOD enzymatic reaction pathway. On the basis of the X-ray crystal structures determined in this study, here we discuss the mechanisms of the first and the second half-reactions brought about by TcDHOD.

Structural Insight into the First Half-Reaction, Dihydroorotate Oxidation. The mechanism of the first half-reaction has been extensively discussed based on kinetic analyses (*21, 23, 24, 26, 47*) and crystal structures (*17, 18, 28, 29*), and Cys130 has been identified as the active site base for *L. lactis* DHODA that abstracts a proton from dihydroorotate C_5. In the crystal structure of the TcDHOD−dihydroorotate complex, Cys130 S_γ is 3.52 Å and 3.59 Å away from dihydroorotate C_5 and water K, respectively (Figure 5A). In addition, the calculated positions of the axial C_5 hydrogen, H_{5a}, and Cys130 S_γ hydrogen, H_S, are favorably disposed for the $H_2O^K\cdots H_S-S_\gamma\cdots H_{5a}-C_5$ interaction, as indicated by the distances $S_\gamma-H_{5a}$ (2.54 Å) and $H_S-O^KH_2$ (2.32 Å), and by the angles $S_\gamma-H_{5a}-C_5$ (157.5°) and $S_\gamma-H_S-O^KH_2$ (148.8°). The water K is linked to outside solvents through a hydrogen bond chain formed by three water molecules that are located in a hydrophilic channel connecting Cys130Sγ

to the outside. This channel is also found in family 1A DHODs (2B4G and 2DOR), but it is not found in the K213E mutant of *L. lactis* DHODA (1JQV), in which the active site loop closes the channel. Family 1B DHOD from *L. lactis* (1EP2) does not have this hydrophilic channel; instead, the active site Cys135 is on the molecular surface. Because of this exquisite disposition of Cys130 and the hydrogen bond chain, dihydroorotate H_{5a} would be abstracted by Cys130 as a proton and then relayed to an outside solvent through the hydrogen bond chain.

Together with the proton abstraction from C_5, dihydroorotate H_6 is transferred to FMN N_5 as a hydride (or a hydride equivalent) to reduce the cofactor. As mentioned above in the Results section, the calculated position of H_6 (between C_6 and FMN N_5, 2.19 Å away from FMN N_5, with a $C_6-H_5-N_5$ angle of 160°) is suitably disposed for the hydride transfer. The structure of the TcDHOD−dihydroorotate complex shows that the reduced FMN cofactor is essentially planar, which indicates that it is not neutral reduced FMN, $FMNH_2$, but anionic reduced FMN, $FMNH^-$ (*48*). The negative charge of the anionic reduced FMN is stabilized by Lys43 and Lys164 (Figure 5A). Lys164 is part of the hydrogen bond network of Glu125···H_2O^J···Lys164··· FMN. Although both Glu125 and Lys164 are shielded from outside solvents, a proton would be shifted from the Glu125 carboxyl group to the Lys164 amino group through the hydrogen bond network. Both of the residues are conserved only in the amino acid sequences of DHODs from families 1A and 1B (Figure 1), but inspections of the crystal structures of family 2 DHODs show that alternative glutamate and lysine residues conserved in amino acid sequences of family 2 DHODs (for example, *H. sapiens* DHOD Glu116 and Lys255) similarly form the hydrogen bond network of Glu116···H_2O···Lys255···FMN.

In summary, the first half-reaction proceeds as follows (Figure 5A). After binding of dihydroorotate to TcDHOD, a hydride (or a hydride equivalent) is transferred from dihydroorotate C_6 to FMN N_5, and Cys130 S_γ completes oxidation of dihydroorotate by abstracting a proton from C_5, which is relayed to an outside solvent via the H_2O^K ···H_S-S_γ···$H_{5a}-C_5$ network. The negative charge of the anionic reduced FMN is stabilized by Lys43 and Lys164. This mechanism is consistent with previous works (*18, 23*−*26, 28*−*30*). Although we cannot be sure whether the scission of C_6-H_6 and C_5-H_{5a} bonds is concerted or stepwise, and we cannot be sure whether H_6 is transferred to FMN N_5 as a hydride or a hydride equivalent, the concerted mechanism with the transfer of a hydride equivalent has been proposed for family 1 DHODs (*23*).

Structural Insight into the Second Half-Reaction, Fumarate Reduction. Unlike the physiological substrate of the first half-reaction, those of the second half-reaction differ among the DHOD subfamilies. The reduced FMN cofactor for TcDHOD converts fumarate to succinate, whereas NAD^+ is reduced to NADH by family 1B DHODs, and ubiquinone is reduced to ubiquinol by family 2 DHODs.

The prominent feature we found in the TcDHOD−fumarate complex is that the conformation of the bound fumarate is nonplanar. The second carboxyl group is twisted around the C_3-C_4 bond with a $C_2-C_3-C_4-O_4$ dihedral angle of 99.1° as observed in the bound succinate, dihydroorotate, orotate and oxonate structures. The bound fumarate is twisted by interactions with Lys43 N_ζ, Leu71 N, Gly70 N, and Asn132 $N_{\delta 2}$ (Figure 4D). Twisting around the C_3-C_4 bond breaks the uniform distribution of π-electrons over the conjugated double bonds of fumarate, and partial charge separation, represented as $C_2^{\delta-}$ and $C_3^{\delta+}$, is then induced. Together with the shorter distances of $C_2^{\delta-}$−Cys130 Sδ (3.43 Å) and $C_3^{\delta+}$−FMN N_5 (3.15 Å) than those of $C_3^{\delta+}$− Cys130 Sδ (4.24 Å) and $C_2^{\delta-}$− FMN N_5 (4.03 Å), this partial charge separation may act as a guide, leading a hydride (or hydride equivalent) from FMN N_5 to $C_3^{\delta+}$ and a proton from Cys130 S_γ to $C_2^{\delta-}$ in the thermodynamically favorable reduction of fumarate with reduced FMN. In the same manner as the TcDHOD−dihydroorotate complex, the water K (Figure 5B) was also in the $2F_o - F_c$ electron density map of the TcDHOD−fumarate complex (Supporting Information Figure S2J), and acts a part of the hydrogen bond network $HO^K-H\cdots S_\gamma-H_s\cdots C_2^{\delta-}$. Therefore, a proton can be relayed from an outside solvent to $C_2^{\delta-}$ through the network (Figure 5B).

To find out whether this fumarate twisting is common, we searched the Protein Data Bank for protein structures with fumarate. Ten structures were found. Four [1D4E (*49*), 1P2E (*50*), 2BS2 (*51*), and 1QLB (*52*)] are flavoproteins with fumarate reductase activity, and six [1PJ2 (*53*), 1QCO (*54*), 2CGO (*55*), 2EEO (not published), 2PTQ (*56*), and 2VD6 (not published)] are enzymes in which fumarate is a product (1QCO, 2PTQ, 2VD6), an inhibitor (2CGO, 2EEO), or an allosteric activator (1PJ2). Twisted fumarate is near the isoalloxazine in all fumarate reductases except 2BS2, while a planar fumarate is bound to the other six. Unlike TcDHOD, the distances between $C_2^{\delta-}$ and N_5 (3.38 to 3.96 Å) are comparable with those between $C_3^{\delta+}$ and N_5 (3.35 to 3.89 Å) in 1D4E, 1P2E and 1QLB. Both 2BS2 and 1QLB are quinol:fumarate oxidoreductase from *Wolinella succinogenes*, but 2BS2, in which the active site loop is half-open, is probably unreactive. While the number of examples is small, we speculate that the twisting of fumarate is common in flavoproteins with fumarate reductase activity.

In summary, at atomic resolution we determined the three-dimensional structures of TcDHOD in ligand-free form and in complexes with dihydroorotate, orotate, oxonate, fumarate, and succinate. All structures are essentially identical and include a planar FMN cofactor. The planar reduced FMN cofactor of TcDHOD−dihydroorotate complex indicates that the cofactor is in the form of the anionic reduced FMN. Taking these structures as models of the enzymatic pathway gives insight regarding the catalytic mechanisms of dihydroorotate oxidation and fumarate reduction. We expect that information about the structure of TcDHOD obtained in this study, particularly about interactions between the enzyme and the inhibitor and physiological substrates, will be useful in the design specific and effective inhibitors against TcDHOD.

ACKNOWLEDGMENT

We thank all staff members at beamlines BL44XU at SPring-8 and NW12 at Photon Factory for their help with X-ray diffraction data collection and T. Nakazawa (Nara Women's University) for helpful discussions.

SUPPORTING INFORMATION AVAILABLE

One purification table of recombinant TcDHOD (Table S1), a figure (S1) explaining the pyrimidine *de novo* biosynthesis as well as fumarate and succinate metabolism in *T. cruzi* and a figure (S2) showing detailed electron density map of all ligands complexed with TcDHOD. This material is available free of charge via the Internet at http://pubs.acs.org.

REFERENCES

1. Jensen, K. F., and Bjornberg, O. (1998) Evolutionary and functional families of dihydroorotate dehydrogenases. *Paths Pyrimidines 6*, 20–28.
2. Baldwin, J., Farajallah, A. M., Malmquist, N. A., Rathod, P. K., and Phillips, M. A. (2002) Malarial dihydroorotate dehydrogenase. Substrate and inhibitor specificity. *J. Biol. Chem. 277*, 41827–41834.
3. Gero, A. M., and O'Sullivan, W. J. (1985) Human spleen dihydroorotate dehydrogenase: properties and partial purification. *Biochem. Med. 34*, 70–82.
4. Norager, S., Jensen, K. F., Bjornberg, O., and Larsen, S. (2002) *E. coli* dihydroorotate dehydrogenase reveals structural and functional distinctions between different classes of dihydroorotate dehydrogenases. *Structure 10*, 1211–1223.
5. Liu, S., Neidhardt, E. A., Grossman, T. H., Ocain, T., and Clardy, J. (2000) Structures of human dihydroorotate dehydrogenase in complex with antiproliferative agents. *Structure 8*, 25–33.
6. Marcinkeviciene, J., Rogers, M. J., Kopcho, L., Jiang, W., Wang, K., Murphy, D. J., Lippy, J., Link, S., Chung, T. D., Hobbs, F., Haque, T., Trainor, G. L., Slee, A., Stern, A. M., and Copeland, R. A. (2000) Selective inhibition of bacterial dihydroorotate dehydrogenases by thiadiazolidinediones. *Biochem. Pharmacol. 60*, 339–342.
7. Copeland, R. A., Marcinkeviciene, J., Haque, T. S., Kopcho, L. M., Jiang, W., Wang, K., Ecret, L. D., Sizemore, C., Amsler, K. A., Foster, L., Tadesse, S., Combs, A. P., Stern, A. M., Trainor, G. L., Slee, A., Rogers, M. J., and Hobbs, F. (2000) *Helicobacter pylori*-selective antibacterials based on inhibition of pyrimidine biosynthesis. *J. Biol. Chem. 275*, 33373–33378.
8. Baldwin, J., Michnoff, C. H., Malmquist, N. A., White, J., Roth, M. G., Rathod, P. K., and Phillips, M. A. (2005) High-throughput screening for potent and selective inhibitors of *Plasmodium falciparum* dihydroorotate dehydrogenase. *J. Biol. Chem. 280*, 21847–21853.
9. Heikkila, T., Ramsey, C., Davies, M., Galtier, C., Stead, A. M., Johnson, A. P., Fishwick, C. W., Boa, A. N., and McConkey, G. A. (2007) Design and synthesis of potent inhibitors of the malaria parasite dihydroorotate dehydrogenase. *J. Med. Chem. 50*, 186–191.
10. Palfey, B. A., Bjornberg, O., and Jensen, K. F. (2001) Specific inhibition of a family 1A dihydroorotate dehydrogenase by benzoate pyrimidine analogues. *J. Med. Chem. 44*, 2861–2864.
11. Wolfe, A. E., Thymark, M., Gattis, S. G., Fagan, R. L., Hu, Y. C., Johansson, E., Arent, S., Larsen, S., and Palfey, B. A. (2007) Interaction of benzoate pyrimidine analogues with class 1A dihydroorotate dehydrogenase from *Lactococcus lactis*. *Biochemistry 46*, 5741–5753.
12. Gao, G., Nara, T., Nakajima-Shimada, J., and Aoki, T. (1999) Novel organization and sequences of five genes encoding all six enzymes for de novo pyrimidine biosynthesis in *Trypanosoma cruzi*. *J. Mol. Biol. 285*, 149–161.
13. Nara, T., Hshimoto, T., and Aoki, T. (2000) Evolutionary implications of the mosaic pyrimidine-biosynthetic pathway in eukaryotes. *Gene 257*, 209–222.
14. Takashima, E., Inaoka, D. K., Osanai, A., Nara, T., Odaka, M., Aoki, T., Inaka, K., Harada, S., and Kita, K. (2002) Characterization of the dihydroorotate dehydrogenase as a soluble fumarate reductase in *Trypanosoma cruzi*. *Mol. Biochem. Parasitol. 122*, 189–200.
15. Annoura, T., Nara, T., Makiuchi, T., Hashimoto, T., and Aoki, T. (2005) The origin of dihydroorotate dehydrogenase genes of kinetoplastids, with special reference to their biological significance and adaptation to anaerobic, parasitic conditions. *J. Mol. Evol. 60*, 113–127.
16. Arakaki, T. L., Buckner, F. S., Gillespie, J. R., Malmquist, N. A., Phillips, M. A., Kalyuzhniy, O., Luft, J. R., Detitta, G. T., Verlinde, C. L., Van Voorhis, W. C., Hol, W. G., and Merritt, E. A. (2008) Characterization of *Trypanosoma brucei* dihydroorotate dehydrogenase as a possible drug target; structural, kinetic and RNAi studies. *Mol. Microbiol. 68*, 37–50.
17. Rowland, P., Nielsen, F. S., Jensen, K. F., and Larsen, S. (1997) The crystal structure of the flavin containing enzyme dihydroorotate dehydrogenase A from *Lactococcus lactis*. *Structure 5*, 239–252.
18. Rowland, P., Norager, S., Jensen, K. F., and Larsen, S. (2000) Structure of dihydroorotate dehydrogenase B: electron transfer between two flavin groups bridged by an iron-sulphur cluster. *Structure 8*, 1227–1238.
19. Hurt, D. E., Widom, J., and Clardy, J. (2006) Structure of *Plasmodium falciparum* dihydroorotate dehydrogenase with a bound inhibitor. *Acta Crystallogr., Sect. D: Biol. Crystallogr. 62*, 312–323.
20. Hansen, M., Le Nours, J., Johansson, E., Antal, T., Ullrich, A., Loffler, M., and Larsen, S. (2004) Inhibitor binding in a class 2 dihydroorotate dehydrogenase causes variations in the membrane-associated N-terminal domain. *Protein Sci. 13*, 1031–1042.
21. Bjornberg, O., Jordan, D. B., Palfey, B. A., and Jensen, K. F. (2001) Dihydrooxonate is a substrate of dihydroorotate dehydrogenase (DHOD) providing evidence for involvement of cysteine and serine residues in base catalysis. *Arch. Biochem. Biophys. 391*, 286–294.
22. Bjornberg, O., Rowland, P., Larsen, S., and Jensen, K. F. (1997) Active site of dihydroorotate dehydrogenase A from *Lactococcus lactis* investigated by chemical modification and mutagenesis. *Biochemistry 36*, 16197–16205.
23. Fagan, R. L., Jensen, K. F., Bjornberg, O., and Palfey, B. A. (2007) Mechanism of flavin reduction in the class 1A dihydroorotate dehydrogenase from *Lactococcus lactis*. *Biochemistry 46*, 4028–4036.
24. Fagan, R. L., Nelson, M. N., Pagano, P. M., and Palfey, B. A. (2006) Mechanism of flavin reduction in class 2 dihydroorotate dehydrogenases. *Biochemistry 45*, 14926–14932.
25. Jiang, W., Locke, G., Harpel, M. R., Copeland, R. A., and Marcinkeviciene, J. (2000) Role of lys100 in human dihydroorotate dehydrogenase: mutagenesis studies and chemical rescue by external amines. *Biochemistry 39*, 7990–7997.
26. Jordan, D. B., Bisaha, J. J., and Picollelli, M. A. (2000) Catalytic properties of dihydroorotate dehydrogenase from *Saccharomyces cerevisiae*: studies on pH, alternate substrates, and inhibitors. *Arch. Biochem. Biophys. 378*, 84–92.
27. Marcinkeviciene, J., Jiang, W., Locke, G., Kopcho, L. M., Rogers, M. J., and Copeland, R. A. (2000) A second dihydroorotate dehydrogenase (Type A) of the human pathogen *Enterococcus faecalis*: expression, purification, and steady-state kinetic mechanism. *Arch. Biochem. Biophys. 377*, 178–186.
28. Norager, S., Arent, S., Bjornberg, O., Ottosen, M., Lo Leggio, L., Jensen, K. F., and Larsen, S. (2003) *Lactococcus lactis* dihydroorotate dehydrogenase A mutants reveal important facets of the enzymatic function. *J. Biol. Chem. 278*, 28812–28822.
29. Rowland, P., Bjornberg, O., Nielsen, F. S., Jensen, K. F., and Larsen, S. (1998) The crystal structure of *Lactococcus lactis* dihydroorotate dehydrogenase A complexed with the enzyme reaction product throws light on its enzymatic function. *Protein Sci. 7*, 1269–1279.
30. Mohsen, A. W., Rigby, S. E., Jensen, K. F., Munro, A. W., and Scrutton, N. S. (2004) Thermodynamic basis of electron transfer in dihydroorotate dehydrogenase B from *Lactococcus lactis*: analysis by potentiometry, EPR spectroscopy, and ENDOR spectroscopy. *Biochemistry 43*, 6498–6510.
31. Inaoka, D. K., Takashima, E., Osanai, A., Shimizu, H., Nara, T., Aoki, T., Harada, S., and Kita, K. (2005) Expression, purification and crystallization of *Trypanosoma cruzi* dihydroorotate dehydrogenase complexed with orotate. *Acta Crystallogr., Sect. F: Struct. Biol. Cryst. Commun. 61*, 875–878.
32. Hartree, E. F. (1972) Determination of protein: a modification of the Lowry method that gives a linear photometric response. *Anal. Biochem. 48*, 422–427.
33. Otwinowski, Z., and Minor, W. (1997) Processing of X-ray diffraction data collected in oscillation mode. *Methods Enzymol. 276*, 307–326.
34. Vagin, A., and Teplyakov, A. (1997) MOLREP: an automated program for molecular replacement. *J. Appl. Crystallogr. 30*, 1022–1025.
35. Sariego, I., Annoura, T., Nara, T., Hashimoto, M., Tsubouchi, A., Iizumi, K., Makiuchi, T., Murata, E., Kita, K., and Aoki, T. (2006) Genetic diversity and kinetic properties of *Trypanosoma cruzi* dihydroorotate dehydrogenase isoforms. *Parasitol. Int. 55*, 11–16.

36. Guex, N., and Peitsch, M. C. (1997) SWISS-MODEL and the Swiss-PdbViewer: an environment for comparative protein modeling. *Electrophoresis 18*, 2714–2723.
37. Brunger, A. T., Adams, P. D., Clore, G. M., DeLano, W. L., Gros, P., Grosse-Kunstleve, R. W., Jiang, J. S., Kuszewski, J., Nilges, M., Pannu, N. S., Read, R. J., Rice, L. M., Simonson, T., and Warren, G. L. (1998) Crystallography & NMR system: A new software suite for macromolecular structure determination. *Acta Crystallogr., Sect. D: Biol. Crystallogr. 54*, 905–921.
38. Emsley, P., and Cowtan, K. (2004) Coot: model-building tools for molecular graphics. *Acta Crystallogr. Sect. D: Biol. Crystallogr. 60*, 2126–2132.
39. Murshudov, G. N., Vagin, A. A., and Dodson, E. J. (1997) Refinement of macromolecular structures by the maximum-likelihood method. *Acta Crystallogr., Sect. D: Biol. Crystallogr. 53*, 240–255.
40. Ramachandran, G. N., and Sasisekharan, V. (1968) Conformation of polypeptides and proteins. *Adv. Protein Chem. 23*, 283–438.
41. Laskowski, R. A., MacArthur, M. W., Moss, D. S., and Thornton, J. M. (1993) PROCHECK: a program to check the stereochemical quality of protein structures. *J. Appl. Crystallogr. 26*, 283–291.
42. Collaborative Computational Project, N. 1994, The CCP4 suite: programs for protein crystallography. *Acta Crystallogr., Sect. D: Biol. Crystallogr.* 760–763.
43. Pinheiro, M. P., Iulek, J., and Cristina Nonato, M. (2008) Crystal structure of *Trypanosoma cruzi* dihydroorotate dehydrogenase from Y strain. *Biochem. Biophys. Res. Commun. 369*, 812–817.
44. Bjornberg, O., Gruner, A. C., Roepstorff, P., and Jensen, K. F. (1999) The activity of *Escherichia coli* dihydroorotate dehydrogenase is dependent on a conserved loop identified by sequence homology, mutagenesis, and limited proteolysis. *Biochemistry 38*, 2899–2908.
45. James, M. N., Sielecki, A. R., Brayer, G. D., Delbaere, L. T., and Bauer, C. A. (1980) Structures of product and inhibitor complexes of *Streptomyces griseus* protease A at 1.8 Å resolution. A model for serine protease catalysis. *J. Mol. Biol. 144*, 43–88.
46. Pauling, L. (1960) *The nature of the chemical bond*, 3rd ed., Cornell Univ. Press, Ithaca, NY.
47. Nielsen, F. S., Rowland, P., Larsen, S., and Jensen, K. F. (1996) Purification and characterization of dihydroorotate dehydrogenase A from *Lactococcus lactis*, crystallization and preliminary X-ray diffraction studies of the enzyme. *Protein Sci. 5*, 852–856.
48. Zheng, Y., and Ornstein, R. L. (1996) A theoretical study of the structures of flavin in different oxidation and protonation states. *J. Am. Chem. Soc. 118*, 9402–9408.
49. Leys, D., Tsapin, A. S., Nealson, K. H., Meyer, T. E., Cusanovich, M. A., and Van Beeumen, J. J. (1999) Structure and mechanism of the flavocytochrome *c* fumarate reductase of *Shewanella putrefaciens* MR-1. *Nat. Struct. Biol. 6*, 1113–1117.
50. Rothery, E. L., Mowat, C. G., Miles, C. S., Walkinshaw, M. D., Reid, G. A., and Chapman, S. K. (2003) Histidine 61: an important heme ligand in the soluble fumarate reductase from *Shewanella frigidimarina*. *Biochemistry 42*, 13160–13169.
51. Madej, M. G., Nasiri, H. R., Hilgendorff, N. S., Schwalbe, H., and Lancaster, C. R. (2006) Evidence for transmembrane proton transfer in a dihaem-containing membrane protein complex. *EMBO J. 25*, 4963–4970.
52. Lancaster, C. R., Kroger, A., Auer, M., and Michel, H. (1999) Structure of fumarate reductase from *Wolinella succinogenes* at 2.2 Å resolution. *Nature 402*, 377–385.
53. Tao, X., Yang, Z., and Tong, L. (2003) Crystal structures of substrate complexes of malic enzyme and insights into the catalytic mechanism. *Structure 11*, 1141–1150.
54. Timm, D. E., Mueller, H. A., Bhanumoorthy, P., Harp, J. M., and Bunick, G. J. (1999) Crystal structure and mechanism of a carbon-carbon bond hydrolase. *Structure 7*, 1023–1033.
55. Hewitson, K. S., Lienard, B. M., McDonough, M. A., Clifton, I. J., Butler, D., Soares, A. S., Oldham, N. J., McNeill, L. A., and Schofield, C. J. (2007) Structural and mechanistic studies on the inhibition of the hypoxia-inducible transcription factor hydroxylases by tricarboxylic acid cycle intermediates. *J. Biol. Chem. 282*, 3293–3301.
56. Tsai, M., Koo, J., Yip, P., Colman, R. F., Segall, M. L., and Howell, P. L. (2007) Substrate and product complexes of *Escherichia coli* adenylosuccinate lyase provide new insights into the enzymatic mechanism. *J. Mol. Biol. 370*, 541–554.

BI800413R

Acta Crystallographica Section F
Structural Biology and Crystallization Communications
ISSN 1744-3091
Editors: **H. M. Einspahr and J. M. Guss**

Screening of detergents for solubilization, purification and crystallization of membrane proteins: a case study on succinate:ubiquinone oxidoreductase from *Escherichia coli*

Hironari Shimizu, Coh-ichi Nihei, Daniel Ken Inaoka, Tatushi Mogi, Kiyoshi Kita and Shigeharu Harada

Acta Cryst. (2008). F**64**, 858–862

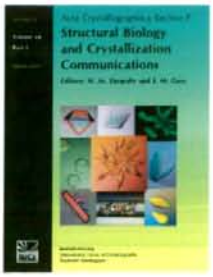

Acta Crystallographica Section F
Structural Biology and Crystallization Communications
ISSN 1744-3091

Screening of detergents for solubilization, purification and crystallization of membrane proteins: a case study on succinate:ubiquinone oxidoreductase from *Escherichia coli*

Hironari Shimizu,[a] Coh-ichi Nihei,[a]‡ Daniel Ken Inaoka,[a] Tatushi Mogi,[a] Kiyoshi Kita[a] and Shigeharu Harada[b]*

[a]Department of Biomedical Chemistry, Graduate School of Medicine, The University of Tokyo, 7-3-1 Hongo, Bunkyo-ku, Tokyo 113-0033, Japan, and [b]Department of Applied Biology, Graduate School of Science and Technology, Kyoto Institute of Technology, Sakyo-ku, Kyoto 606-8585, Japan

‡ Present address: Department of Microbiology, Graduate School of Medicine, The University of Tokyo, 7-3-1 Hongo, Bunkyo-ku, Tokyo 113-0033, Japan.

Correspondence e-mail: harada@kit.ac.jp

Received 19 February 2008
Accepted 18 August 2008

Succinate:ubiquinone oxidoreductase (SQR) was solubilized and purified from *Escherichia coli* inner membranes using several different detergents. The number of phospholipid molecules bound to the SQR molecule varied greatly depending on the detergent combination that was used for the solubilization and purification. Crystallization conditions were screened for SQR that had been solubilized and purified using 2.5%(*w*/*v*) sucrose monolaurate and 0.5%(*w*/*v*) Lubrol PX, respectively, and two different crystal forms were obtained in the presence of detergent mixtures composed of *n*-alkyl-oligoethylene glycol monoether and *n*-alkyl-maltoside. Crystallization took place before detergent phase separation occurred and the type of detergent mixture affected the crystal form.

1. Introduction

Membrane proteins consist of one or more hydrophobic regions that are buried in the membrane as well as hydrophilic regions that contain charged or polar residues that are exposed to water. For crystallization, membrane proteins are usually solubilized from the membranes using a detergent and then purified in the presence of a detergent. The membrane proteins thus prepared are water-soluble protein–detergent complexes in which the membrane-anchored hydrophobic portions are covered with amphiphilic detergent molecules. Crystallization of membrane proteins has been carried out using these protein–detergent complexes. Since the successful crystallization of bacteriorhodopsin (Michel & Oesterheld, 1980) and porin (Garavito & Rosenbusch, 1980) in 1980, many membrane proteins have been crystallized and there are currently 167 unique structures (http://blanco.biomol.uci.edu/Membrane_Proteins_xtal.html) in the Protein Data Bank. However, the crystallization of membrane proteins is still a difficult task and the quality of the crystals obtained has often been insufficient for X-ray diffraction studies. One of the obstacles in the crystallization of membrane proteins is that detergents suitable for solubilization, purification and crystallization must be found by trial and error.

Succinate:ubiquinone oxidoreductase (SQR) is a member of the citric acid cycle and catalyzes the oxidation of succinate to fumarate in conjunction with the reduction of ubiquinone to ubiquinol during aerobic respiration. The enzyme from *Escherichia coli* inner membranes consists of four subunits with five prosthetic groups: one covalently bound FAD, three Fe–S clusters and one haem *b*. The flavoprotein subunit (70 kDa) and Fe–S-containing subunit (30 kDa) are hydrophilic and contain all of the prosthetic groups except for the haem *b*, which is contained in two smaller membrane-anchoring subunits (14 and 13 kDa). As *E. coli* SQR can easily be purified in large quantities according to an established method (Kita *et al.*, 1989) and the X-ray structure has already been determined by Yankovskaya *et al.* (2003) at 2.6 Å resolution, the enzyme appears to be suitable for studies of membrane-protein crystallization. In this work, the phospholipid contents of *E. coli* SQR preparations obtained after solubilization and purification using different detergents were analyzed. Screening of crystallization conditions was performed for

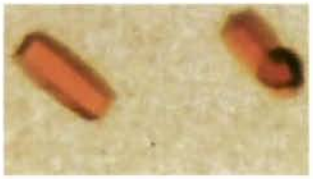

SQR that was prepared using sucrose monolaurate and Lubrol PX for solubilization and purification, respectively, and two new crystal forms were obtained in the presence of detergent mixtures composed of *n*-alkyl-oligoethylene glycol monoether and *n*-alkyl-maltoside.

2. Methods

2.1. Expression and preparation of membranes

A *Bam*HI fragment (*sdhCDAB*) was inserted into pLC339 vector as described by Kita *et al.* (1989). The plasmid was introduced into *E. coli* K12 strain ST4785/pGS133, which lacks the cytochrome *bo* operon. Cells were grown aerobically at 310 K in a 10 l jar fermentor containing LB medium (Miller, 1972) and kanamycin (50 mg l^{-1}) under vigorous agitation and aeration. The addition of kanamycin was essential for the overproduction of *E. coli* SQR, which was at least sixfold higher than in the wild-type strain. The cells were harvested in the late exponential phase of growth and washed in 50 m*M* Tris–HCl buffer pH 7.4 containing 3 m*M* EDTA and 0.1 m*M* PMSF. The typical yield was about 200 g of wet cells from 10 l of culture. Membrane vesicles were prepared from freshly grown cells (200 g) suspended in 500 ml 50 m*M* Tris–HCl buffer pH 7.4 containing 20 m*M* EDTA and a protease-inhibitor cocktail (Sigma) by EDTA/lysozyme treatment followed by disruption with a French press (Yamato *et al.*, 1975). After the removal of any unbroken cells by low-speed centrifugation, membranes were pelleted by ultracentrifugation at 200 000*g* for 2 h at 277 K. The pellet was suspended in 600 ml buffer solution (50 m*M* Tris–HCl pH 7.4 and 10 m*M* EDTA) and the suspension (25 ml) loaded onto buffer (50 ml) containing 44%(*w*/*v*) sucrose was centrifuged at 200 000*g* for 2 h in a Hitachi P45AT fixed-angle rotor. The reddish-brown coloured band of membranes which formed in the middle of the ultracentrifugation tube was separated from the white pellet. The membrane fraction was diluted four times with the buffer and then precipitated by centrifugation at 200 000*g* for 2 h. The pellet was resuspended in a minimum amount of buffer (~80 ml) containing 10%(*w*/*v*) sucrose.

2.2. Estimation of SQR concentration

Since the absorbances at 280 nm (A_{280}s) of the detergents and chemicals in the buffer solutions used in this study were small, the concentration of the *E. coli* SQR was estimated using the calculated molar extinction coefficient at 280 nm (ε_{280} = 129 440), giving A_{280} = 10.6 for a pure SQR solution at 10 mg ml^{-1}. The ε_{280} value was calculated using $\varepsilon_{280} = 5690n_x + 1280n_y$ (Edelhoch, 1967), where 5690 and 1280 are the molar absorption coefficients at 280 nm of tryptophan and tyrosine and n_x and n_y are the number of tryptophan and tyrosine residues in *E. coli* SQR, respectively.

2.3. Assay for phospholipid content

The phospholipid content was assayed using the Fiske–SubbaRow method (Bartlett, 1959). A suitable quantity of the membrane suspension or purified SQR preparation was mixed with 0.5 ml 10 *N* H_2SO_4 in a clean glass test tube and heated in an oven at 423–433 K for more than 3 h. Organic compounds were dehydrated and decomposed to carbon by the H_2SO_4 and the inorganic phosphorus was liberated from the phospholipid. After the addition of several drops of 30% H_2O_2, the solution was again heated (423–433 K) for at least 1.5 h. 4.6 ml 0.22%(*w*/*v*) ammonium molybdate and 0.2 ml of the Fiske–SubbaRow reagent (Bartlett, 1959) were added to the solution, mixed thoroughly and heated for 7 min in a boiling water bath. The colourless solution turned blue and the absorbance at 830 nm (A_{830}) was measured. The concentration of the phosphorus liberated from the phospholipid was estimated from the A_{830} values of standard solutions containing an inorganic phosphate compound of known concentration. For simplicity, we assumed that the phospholipid contained only one P atom unless described otherwise. The A_{830} given by 0.02 µmol PO_4^{3-} is about 0.2 and thus 1 mg of SQR (0.008 µmol) with one bound phospholipid molecule produces an A_{830} of about 0.08. The concentration of the phospholipid in the membrane suspension prepared as described above was about 20 m*M*.

2.4. Solubilization and purification of SQR

In this study, two new crystal forms of *E. coli* SQR were obtained using a preparation that was solubilized from the membranes using 2.5%(*w*/*v*) sucrose monolaurate (CMC = 0.4 m*M*; Dojindo) and purified in the presence of 0.5%(*w*/*v*) Lubrol PX (Nacalai Tesque). Lubrol PX, which is a cheaper detergent than sucrose monolaurate, is a mixture of C_nH_{2n+1}-$(OCH_2CH_2)_m$-OH (abbreviated as C_nE_m) with different-length hydrocarbon and ethylene glycol chains and is virtually the same detergent as THESIT used by Yankovskaya *et al.* (2003). The membrane suspension prepared from 100 g of *E. coli* cells was diluted with buffer solution (20 m*M* Tris–HCl pH 7.4, 10 m*M* $MgCl_2$ and 2 m*M* sodium malonate) to give a phospholipid concentration of 4 m*M* and a freshly prepared 25%(*w*/*v*) sucrose monolaurate solution (477 m*M*) was stirred into the suspension until a final concentration of 2.5%(*w*/*v*) was achieved. After stirring for 1 h at 277 K, the solution was centrifuged at 200 000*g* for 1 h. The clear reddish-brown supernatant containing the solubilized SQR was applied onto a column of GE Healthcare DEAE Sepharose FF (500 ml bed volume) equilibrated with buffer *A* [20 m*M* Tris–HCl pH 7.4, 2 m*M* sodium malonate and 0.5%(*w*/*v*) Lubrol PX]. After washing the column with 2000 ml buffer *A*, SQR was eluted with 4000 ml of buffer *A* containing a linear gradient of 0.0–0.3 *M* NaCl. Fractions containing SQR (A_{412}/A_{280} > 0.5; Fig. 1, lane 1) were pooled. Solid polyethylene glycol 3350 (PEG 3350) was gradually added (30 g per 100 ml) to the pooled fraction containing about

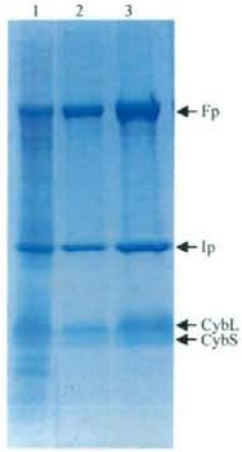

Figure 1
A 12% SDS–PAGE gel stained with Coomassie Brilliant Blue showing the purity of the purified *E. coli* SQR. Lane 1, an eluted fraction from DEAE Sepharose FF; lane 2, an eluted fraction from Source 15Q; lane 3, the purified SQR after sucrose density-gradient ultracentrifugation. Hydrophilic (Fp and Ip) and hydrophobic (CybL and CybS) subunits are shown by arrows.

Table 1
Average number of phospholipid molecules bound to purified SQR.

The *E. coli* SQR was solubilized using 0.1% (1.9 m*M*), 1.0% (19 m*M*), 2.5% (48 m*M*) and 4.0% (76 m*M*) sucrose monolaurate from membranes with different phospholipid concentrations and purified in the presence of 0.5%(*w*/*v*) Lubrol PX. Values in parentheses are the molar ratios of SML to phospholipid in the membrane suspension.

SML† concentration (m*M*)	Phospholipid concentration in membrane suspension (m*M*)	Average No. of phospholipids per SQR monomer‡§
1.9 (4.8)	0.4	11
19 (0.95)	20	10
19 (4.8)	4.0	8
48 (3.0)	12	6
48 (12)¶	4.0	6
48 (24)	2.0	6
76 (3.8)	20	6
76 (19)	4.0	6

† Sucrose monolaurate (CMC 0.4 m*M*). ‡ The concentration of the purified SQR was estimated by A_{280} (A_{280} = 10.6 for 10 mg ml^{-1} SQR solution). § It was assumed that the phospholipid contained only one P atom. ¶ Crystallization was performed for SQR solubilized under this condition.

530 mg SQR and the pellet obtained by centrifugation was dissolved again in buffer *A*. Residual impurities were successfully removed using a GE Healthcare Source 15Q column (70 ml bed volume). Fractions with an $A_{412}/A_{280} > 0.6$ obtained by elution with 1000 ml of a linear gradient of 0–0.3 *M* NaCl were pooled (Fig. 1, lane 2). The purified SQR (200 mg) was then subjected to sucrose density-gradient ultracentrifugation. The pooled SQR was precipitated by adding solid PEG 3350 and dissolved again in a minimum amount of buffer *A* (~4 ml). The SQR solution (2 ml) was carefully loaded onto buffer *A* (~73 ml) containing a 6–40%(*w*/*v*) sucrose-density gradient and centrifuged at 200 000*g* overnight in a Hitachi P45AT fixed-angle rotor. The SQR, which focused as a deep reddish-coloured sharp band in the middle of the gradient (Fig. 1, lane 3), was separated from the broad pale-reddish upper half in approximately 95% yield, precipitated by PEG 3350 and stored at 193 K for subsequent use. Sodium malonate, an inhibitor of SQR, was added to all of the purification and crystallization steps in order to stabilize the enzyme.

2.5. Detergent exchange

Detergent exchange was performed at 277 K as follows. After purification in the presence of Lubrol PX, the SQR precipitated by PEG 3350 was dissolved in 20 m*M* Tris–HCl buffer pH 7.4 containing 2 m*M* sodium malonate, 200 m*M* KCl and 1% of the detergent of choice. The A_{280} of the SQR solution was set to about 10. After incubation for 20 min on ice, the enzyme was precipitated by adding a 1.4-fold volume of 40%(*w*/*w*) PEG 3350 when the type of detergent exchanged was an *n*-alkyl-oligoethylene glycol monoether (C_nE_m). The pellet obtained by centrifugation was again dissolved in the same buffer and the enzyme was precipitated by PEG 3350 after a 20 min incubation period. This procedure was repeated several times. Exchanges to *n*-alkyl-glucosides (C_nG) and *n*-alkyl-maltosides (C_nM) were performed similarly, but the enzyme was precipitated by adding a 1.2-fold volume of 4.0 *M* ammonium sulfate. Since ammonium sulfate can cause phase separation of a solution containing C_nE_m and PEG can cause phase separation of a solution containing C_nG or C_nM, an appropriate choice of precipitants should be made in order to avoid the denaturation of the enzyme caused by phase separation. The completeness of detergent exchange was checked by thin-layer chromatography (Reiss-Husson, 1992).

Table 2
Average number of phospholipid molecules bound to purified SQR.

The *E. coli* SQR was solubilized and purified using different combinations of detergents. The concentration of phospholipids in the membranes was 4 m*M*, assuming that the phospholipid contained only one P atom.

Detergent used for			
Solubilization (2.5%)	Purification (0.5%)	Average No. of phospholipids per SQR monomer†	Crystallization‡
LDAO§	LDAO	~100	Failed
DOC¶	LDAO	~100	Failed
DOC	SMC††	19	Failed
SMC	SMC	16	Failed
SML‡‡	SML	6	Successful
SML	Lubrol PX§§	6	Successful
Lubrol PX	Lubrol PX	24	Failed
Lubrol PX (4%)	Lubrol PX	6	Successful

† The concentration of the purified SQR was estimated by A_{280} (A_{280} = 10.6 for 10 mg ml^{-1} SQR solution). ‡ Results of crystallization trials according to the optimized procedure described in the text. § *N*,*N*-Dimethyldodecylamine-*N*-oxide (CMC 1.4 m*M*, 0.03%). ¶ Deoxycholic acid (CMC 5 m*M*, 0.2%). †† Sucrose monocaprate (CMC 2.5 m*M*, 0.13%). ‡‡ Sucrose monolaurate (CMC 0.4 m*M*, 0.02%). §§ C_nH_{2n+1}-$(OCH_2CH_2)_m$-OH (n = 12, 14; m = 9.5).

2.6. Crystallization and X-ray diffraction experiments

Crystallization conditions were screened by the hanging-drop vapour-diffusion technique using 96-well CrystalClear Strips (Hampton Research). The SQR was dissolved in 10 m*M* Tris–HCl pH 7.6 buffer containing 2 m*M* sodium malonate and the detergent of choice (A_{280} = 30) and centrifuged for 20 min at 20 000*g* to remove any undissolved material. To set up the hanging-drop vapour diffusion, a droplet made up of 0.5 µl SQR solution and 0.5 µl reservoir solution was incubated over a well containing 100 µl reservoir solution. Initial screening was carried out at 277 and 293 K using the commercially available crystallization kits Crystal Screen (Jancarik & Kim, 1991) and Crystal Screen II from Hampton Research.

X-ray diffraction experiments were performed using the synchrotron beamlines BL44XU at SPring-8 (Harima, Japan), BL-5A at PF and NW12A at PF-AR (Tsukuba, Japan). For X-ray diffraction experiments at 100 K, crystals were transferred to reservoir solution supplemented with 15% glycerol and then frozen by rapid submergence in liquid nitrogen. The data were processed and scaled using programs from the *HKL*-2000 suite (Otwinowski & Minor, 1997).

3. Results and discussion

3.1. Phospholipid content of purified SQR

Since the major constituent (~80% in weight) of the *E. coli* inner membranes is phospholipids (Tanford, 1980), the phospholipid content is a good indicator of the amount of lipid bound to the purified SQR. After solubilization from the membranes using 2.5%(*w*/*v*) sucrose monolaurate and purification in the presence of 0.5%(*w*/*v*) Lubrol PX as described in §2, the concentration of the phosphorus liberated from the phospholipid molecules bound to the purified SQR was measured. Assuming that the phospholipid molecules bound to the purified SQR contained one P atom and that the A_{280} of the 10 mg ml^{-1} SQR solution was 10.6, six bound phospholipid molecules per SQR monomer were detected. The phospholipid contents of SQR prepared under different solubilization conditions were also analyzed. Solubilization with 2.5%(*w*/*v*) or 4.0%(*w*/*v*) sucrose monolaurate gave a value of six regardless of the molar ratio between the detergent and phospholipid in the membrane suspension, whereas the phospholipid content increased to 11 on a decrease in the sucrose monolaurate concentration (Table 1). Therefore, these

six phospholipid molecules seem to be more tightly bound to the SQR. We also performed solubilization and purification using other commercially available detergents (Table 2). *N*,*N*-Dimethyldodecylamine-*N*-oxide (Fluka) and deoxycholic acid (Wako) produced SQR preparations containing ~100 phospholipid molecules. However, the phospholipid content was reduced to 19 when purification was performed in the presence of 0.5%(*w*/*v*) sucrose monocaprate (Dojindo). Accordingly, most of the phospholipid molecules were loosely bound to the SQR and were removed by the action of 0.5%(*w*/*v*) sucrose monocaprate. On the other hand, 2.5%(*w*/*v*) and 4%(*w*/*v*) Lubrol PX gave phospholipid contents of 24 and six, respectively. In the X-ray structure of *E. coli* SQR solubilized using 4% THESIT, which is virtually the same detergent as Lubrol PX, two well ordered phospholipid molecules, phosphatidylethanolamine and cardiolipin, were found per SQR monomer (Yankovskaya *et al.*, 2003). Since phosphatidylthanolamine and cardiolipin contain one and two P atoms, respectively, there are three P atoms per SQR monomer in the X-ray structure. The disagreement over the number of P atoms probably arises from two causes. Firstly, since the concentration of the SQR was estimated from the calculated molar extinction coefficient in this study, the number of P atoms determined are relative rather than absolute values. Secondly, there may be additional disordered phospholipid molecules which are not detected by X-ray analysis.

Since the Fiske–SubbaRow method only gives an average phospholipid content, it is not known whether or not the purified SQR was uniform in the number of bound phospholipid molecules. Following the Source 15Q column, the purified SQR with six bound phospholipid molecules was subjected to sucrose density-gradient ultracentrifugation at 200 000*g* overnight. After centrifugation, most of the SQR (about 95%) was focused in a sharp deep-reddish band which formed in the middle of the gradient, with a small amount of the enzyme (about 4%) spread broadly at the upper part of the gradient. The phospholipid content of the SQR in the sharp band was six, but in the broad band the phospholipid content was in the range 10–15 depending on the position of the gradient. This result indicates that the uniformity in the phospholipid content was improved by sucrose density-gradient ultracentrifugation.

3.2. Crystallization

After solubilization and purification using 2.5%(*w*/*v*) sucrose monolaurate and 0.5%(*w*/*v*) Lubrol PX, respectively, the purified SQR dissolved in 10 m*M* Tris–HCl buffer pH 7.4 containing 2 m*M* sodium malonate and 0.5%(*w*/*v*) Lubrol PX (50 mg ml^{-1} protein) was subjected to a crystallization trial using commercially available screening kits. Aggregates of small crystals were observed in a large amount of amorphous precipitate using several reservoir solutions containing PEG as a precipitant. An attempt was made to optimize the crystallization conditions by using PEGs with different molecular weights and by varying the PEG concentration, the pH and the temperature. However, none of the conditions investigated improved the results. Since Lubrol PX is a heterogeneous detergent, the detergent was exchanged for commercially available synthetic homogeneous $C_{12}E_8$ and $C_{10}E_8$ (Fluka) and the screening was carried out again. However, no single crystals other than aggregates of small crystals were observed. Additive Screen kits (Hampton Research) were used to examine the effects of adding various compounds but also failed. Single crystals of *E. coli* SQR were finally obtained when either *n*-dodecyl-β-D-maltoside (C_{12}M, Dojindo) or *n*-decyl-β-D-maltoside (C_{10}M, Dojindo) was used as an additive, but their optimum quantities varied subtly from experiment to experiment.

To attain reproducible crystallization, the Lubrol PX in the purified SQR was exchanged for detergent mixtures composed of $C_{12}E_8$ and C_{12}M in ratios of 10:0, 9:1, 8:2 and 7:3 (by weight). Exchange to detergent mixtures with higher C_{12}M content denatured the SQR and the addition of PEG 3350 caused phase separation of the SQR solutions, in which the SQR was concentrated in the phase enriched with the detergent. After detergent exchange, the enzyme was dissolved in 10 m*M* Tris–HCl pH 7.4 and 2 m*M* sodium malonate solution containing $C_{12}E_8$ and C_{12}M in the prescribed ratio with a total concentration of 0.2%(*w*/*v*) and optimization of the crystallization conditions was repeated. Plate-shaped deep-red crystals with typical dimensions of 0.2 × 0.1 × 0.02 mm (Fig. 2*a*) appeared reproducibly within 3 d from reservoir solution composed of 16%(*w*/*v*) PEG 3350, 100 m*M* Tris–HCl pH 8.0, 2 m*M* sodium malonate and 200 m*M* KCl at 293 K when the ratio of $C_{12}E_8$ and C_{12}M was 8:2 (by weight).

Since it has been noted that phase separation plays a major role in the crystallization of membrane proteins (Garavito & Picot, 1990; Reiss-Husson, 1992), the concentrations of PEG 3350 that caused phase separation of solutions containing $C_{12}E_8$ and C_{12}M with a total concentration of 0.2% were examined at 293 K. The 10:0 solution, which contained only 0.2%(*w*/*v*) $C_{12}E_8$ in 100 m*M* Tris–HCl pH 8.0, 2 m*M* sodium malonate and 200 m*M* KCl, separated into two phases at 28%(*w*/*v*) PEG 3350. However, as the ratio of C_{12}M increased, the concentration of PEG 3350 required gradually decreased to 23% and finally to 7%(*w*/*v*) PEG 3350 at 8:2 and 0:10, respectively. Therefore, the crystallization of *E. coli* SQR seems to take place using the 8:2 mixed detergent because the PEG 3350 concentrations necessary for crystallization and phase separation are closer to each other at 8:2 than those observed for the other mixed detergents with lower C_{12}M contents. Interestingly, crystals of the same quality were also obtained at 7.5:2.5, but microcrystals formed only occasionally at 8.5:1.5. Crystals of the same crystal form were also obtained under a similar crystallization condition (20% PEG 3350, 100 m*M* Tris–HCl pH 8.2, 2 m*M* malonate and 200 m*M* KCl at 293 K) using an 8:2 mixture of $C_{12}E_8$ and C_{10}M. X-ray diffraction experiments were performed under liquid-nitrogen-cooled conditions at 100 K using synchrotron radiation. Although fresh crystals diffracted to better than 3 Å resolution, the diffraction limits rapidly reduced to lower than 4 Å resolution owing to radiation damage. Analysis of the symmetry and systematic absences of diffraction patterns indicated that the crystals belonged to the monoclinic space group $P2_1$, with unit-cell para-

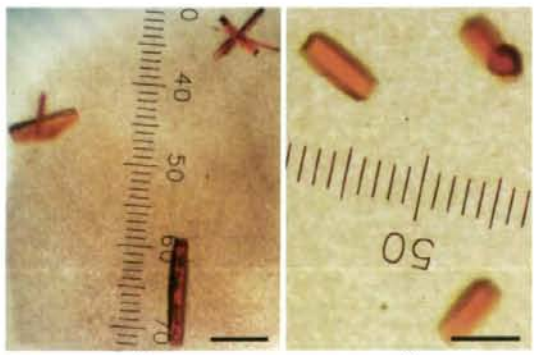

(*a*) (*b*)

Figure 2
Crystals of *E. coli* SQR obtained using (*a*) 0.16% $C_{12}E_8$ and 0.04% C_{12}M and (*b*) 0.16% $C_{10}E_8$ and 0.04% C_{10}M. The scale bar represents 0.2 mm.

Table 3
Statistics of data collection and processing.

Values in parentheses are for the highest resolution shell.

Wavelength (Å)	1.000
Space group	$P4_122$ (or $P4_322$)
Unit-cell parameters	
a (Å)	121.8
b (Å)	121.8
c (Å)	633.4
Solvent content† (%)	62
Resolution range (Å)	40.0–2.9 (3.04–2.9)
No. of reflections	880368
Unique reflections	86980
Completeness (%)	82.0 (85.6)
R_{merge}‡ (%)	8.2 (49.9)
$I/\sigma(I)$	17.1 (3.7)

† Assuming the presence of three molecules in the asymmetric unit. ‡ $R_{merge} = \sum_{hkl}\sum_i |I_i(hkl) - \langle I(hkl)\rangle| / \sum_{hkl}\sum_i I_i(hkl)$.

meters $a = 121.3$, $b = 186.3$, $c = 216.4$ Å, $\beta = 90.6°$. Assuming six SQR molecules (120 kDa × 6) per asymmetric unit, the V_M value (Matthews, 1968) is calculated to be 3.4 Å^3 Da^{-1} with an estimated solvent content of 64%, which is comparable to that found in previous work (69%) by Yankovskaya *et al.* (2003).

In contrast, enzyme for which the detergent was exchanged from Lubrol PX to an 8:2 mixture of $C_{10}E_8$ and either $C_{12}M$ or $C_{10}M$ crystallized in a different crystal form at 293 K from a reservoir solution composed of 20% PEG 3350, 100 m*M* Tris–HCl pH 8.0, 2 m*M* sodium malonate and 200 m*M* KCl (Fig. 2*b*). Diffraction patterns were recorded on the BL44XU beamline of SPring-8 using a DIP6040 detector at a wavelength of 0.9 Å. The crystals belonged to the tetragonal space group $P4_122$ (or $P4_322$), with unit-cell parameters $a = b = 121.8$, $c = 633.4$ Å. Three SQR molecules per asymmetric unit gave a V_M value of 3.3 Å^3 Da^{-1} and an estimated solvent content of 62%. A total of 880 368 observed reflections were merged to 86 980 unique reflections in the 40.0–2.9 Å resolution range. The data-collection and processing statistics are summarized in Table 3. An attempt to solve the structure using the molecular-replacement method with the *MOLREP* program (Navaza, 1994) as implemented in the *CCP*4 package (Collaborative Computational Project, Number 4, 1994) was carried out using the refined coordinates of *E. coli* SQR (PDB code 1nek). A solution with a trimer structure, which was consistent with the previous work of Yankovskaya *et al.* (2003), was obtained in space group $P4_322$. The trimer model was subsequently subjected to rigid-body refinement and gave an R factor of 39%. However, further refinement is not straightforward: the phospholipid molecules were not located currently because the electron densities of the membrane-anchoring hydrophobic regions were faint.

In conclusion, we show that the phospholipid content of purified SQR depends greatly on the detergent used for solubilization and purification and that the enzyme with the fewest bound phospholipid molecules was successfully crystallized in two crystal forms using mixtures of C_nE_m and C_nM. The reaction centre of photosystem II has also been crystallized using detergent mixtures and the role of detergent mixtures in crystallization has been discussed by Rukhman *et al.* (2000). On the basis of the knowledge obtained in this study, we have succeeded in the crystallization of two membrane proteins, quinol:fumarate reductase from *Ascaris suum* mitochondria and recombinant cyanide-insensitive alternative oxidase from *Trypanosoma brucei*, using different mixtures of detergents (details will be published elsewhere).

We are grateful to the staff members at BL44XU at SPring-8 and NW12 and BL-5A at Photon Factory for their help with X-ray diffraction data collection. This work was supported in part by a grant from Japan Aerospace Exploration Agency (JAXA) and by the Targeted Proteins Research Program (TPRP), by Grants-in-Aid for Scientific Research on Priority Areas, for the 21st Century COE Program (F-3), for Creative Scientific Research from the Japanese Ministry of Education, Science, Culture, Sports and Technology (180 73004, 18GS0314, 1903610) and for Scientific Research (B) from Japan Society for the Promotion of Science (18370042). DKI was a research fellow supported by Japan Society for the Promotion of Science.

References

Bartlett, G. R. (1959). *J. Biol. Chem.* **234**, 466–468.
Collaborative Computational Project, Number 4 (1994). *Acta Cryst.* D**50**, 760–763.
Edelhoch, H. (1967). *Biochemistry*, **6**, 1948–1954.
Garavito, R. M. & Picot, D. (1990). *Methods*, **1**, 57–69.
Garavito, R. M. & Rosenbusch, J. P. (1980). *J. Cell Biol.* **86**, 327–329.
Jancarik, J. & Kim, S.-H. (1991). *J. Appl. Cryst.* **24**, 409–411.
Kita, K., Vibat, C. R. T., Meinhardt, S., Guest, J. R. & Gennis, R. B. (1989). *J. Biol. Chem.* **264**, 2672–2677.
Matthews, B. W. (1968). *J. Mol. Biol.* **33**, 491–497.
Michel, H. & Oesterhelt, M. (1980). *Proc. Natl Acad. Sci. USA*, **77**, 1283–1285.
Miller, J. H. (1972). *Experiments in Molecular Genetics*. New York: Cold Spring Harbor Laboratory Press.
Navaza, J. (1994). *Acta Cryst.* A**50**, 157–163.
Otwinowski, A. & Minor, W. (1997). *Methods Enzymol.* **276**, 307–326.
Reiss-Husson, F. (1992). *Crystallization of Nucleic Acids and Proteins. A Practical Approach*, edited by A. Ducruix & R. Giegé, p. 176. Oxford University Press.
Rukhman, V., Lerner, N. & Adir, N. (2000). *Photosynth. Res.* **65**, 249–259.
Tanford, C. (1980). *The Hydrophobic Effect*, p. 109. New York: Wiley.
Yamato, I., Anraky, Y. & Hirosawa, K. (1975). *J. Biochem. (Tokyo)*, **77**, 705–718.
Yankovskaya, V., Horsefield, R., Törnroth, S., Luna-Chavez, C., Miyoshi, H., Léger, C., Byrne, B., Cecchini, G. & Iwata, S. (2003). *Science*, **299**, 700–704.

Biochimica et Biophysica Acta 1787 (2009) 129–133

Contents lists available at ScienceDirect

Biochimica et Biophysica Acta

journal homepage: www.elsevier.com/locate/bbabio

Antibiotics LL-Z1272 identified as novel inhibitors discriminating bacterial and mitochondrial quinol oxidases

Tatsushi Mogi [a,*], Hideaki Ui [b], Kazuro Shiomi [b], Satoshi Ōmura [b], Hideto Miyoshi [c], Kiyoshi Kita [a]

[a] Department of Biomedical Chemistry, Graduate School of Medicine, The University of Tokyo, Hongo, Bunkyo-ku, Tokyo 113-0033, Japan
[b] Kitasato Institute for Life Sciences and Graduate School of Infection Control Sciences, Kitasato University, Shirokane, Minato-ku, Tokyo 108-8641, Japan
[c] Division of Applied Life Sciences, Graduate School of Agriculture, Kyoto University, Sakyo-ku, Kyoto 606-8502, Japan

ARTICLE INFO

Article history:
Received 9 October 2008
Received in revised form 21 November 2008
Accepted 26 November 2008
Available online 10 December 2008

Keywords:
Quinol oxidase
Inhibitor
Natural antibiotic
Escherichia coli
Trypanosoma brucei
Alternative oxidase

ABSTRACT

To counter antibiotic-resistant bacteria, we screened the Kitasato Institute for Life Sciences Chemical Library with bacterial quinol oxidase, which does not exist in the mitochondrial respiratory chain. We identified five prenylphenols, LL-Z1272β, γ, δ, ε and ζ, as new inhibitors for the *Escherichia coli* cytochrome *bd*. We found that these compounds also inhibited the *E. coli bo*-type ubiquinol oxidase and trypanosome alternative oxidase, although these three oxidases are structurally unrelated. LL-Z1272β and ε (dechlorinated derivatives) were more active against cytochrome *bd* while LL-Z1272γ, δ, and ζ (chlorinated derivatives) were potent inhibitors of cytochrome *bo* and trypanosome alternative oxidase. Thus prenylphenols are useful for the selective inhibition of quinol oxidases and for understanding the molecular mechanisms of respiratory quinol oxidases as a probe for the quinol oxidation site. Since quinol oxidases are absent from mammalian mitochondria, LL-Z1272β and δ, which are less toxic to human cells, could be used as lead compounds for development of novel chemotherapeutic agents against pathogenic bacteria and African trypanosomiasis.

1. Introduction

The emergence of antibiotic-resistant strains of major pathogenic bacteria such as *Staphylococcus aureus* is an increasingly serious public health concern [1]. To evade bacterial drug-resistance mechanisms, new effective chemotherapeutic agents, which have novel mechanisms of action as well as different cellular targets compared with conventional antibiotics, need to be developed [2].

Cytochromes *bo* (CyoABCD) and *bd* (CydAB) are two terminal quinol oxidases of the aerobic respiratory chain in *Escherichia coli* and many other bacteria [3,4 for reviews]. Although they are structurally unrelated, both generate proton-motive force through the oxidation of quinols coupled to dioxygen reduction. Cytochrome *bo* is a proton-pumping heme–copper terminal oxidases and is predominantly expressed under highly aerated growth conditions. In contrast, cytochrome *bd* is a predominant terminal oxidase under microaerophilic growth conditions and performs a variety of physiological functions such as microaerophilic respiration and protection against oxygen stress. Further, cytochrome *bd* and its variant cyanide-insensitive oxidase (CioAB) play a key role in survival and adaptation of pathogenic bacteria that encounter host environments where dioxygen is progressively limited [5–9].

In long slender bloodstream forms of the parasitic protist *Trypanosoma brucei*, which causes sleeping sickness in human and nagana in livestock, mitochondrial respiratory Complexes III and IV are down-regulated and alternative quinol oxidase (AOX) serves as a terminal oxidase [10,11]. AOX is a di-iron family protein bound to the matrix side of the inner membrane and cannot generate the proton-motive force. All three quinol oxidases have no counterparts in mammalian mitochondria, thus they are potential targets for novel antimicrobial chemotherapeutics. In fact, we previously identified ascofuranone (AF), a prenylphenol isolated from a phytopathogenic fungus *Ascochyta viciae* [12], as a potent inhibitor for the growth of *T. brucei* and trypanosome AOX (noncompetitive inhibition with IC_{50} of 2 nM) [13,14].

By screening of hundreds of natural antibiotics in the Kitasato Institute for Life Sciences Chemical Library [15] with the *E. coli* cytochrome *bd*, we found that LL-Z1272γ has potent inhibitory activity. We extended our screening to related compounds and found that antibiotics LL-Z1272β, γ, δ, ε and ζ (Fig. 1), prenylphenols isolated from the fungus *Verticillum* sp. FO-2787 [16], are a unique set of natural compounds that can discriminate and inhibit alternative respiratory quinol oxidases. Thus, antibiotics LL-Z1272 are useful probes for understanding of molecular mechanisms of quinol oxidases and we hope that our findings contribute to the development of new antibiotics.

2. Materials and methods

2.1. Isolation or source of antibiotics and inhibitors

LL-Z1272β, γ, δ, ε and ζ were isolated from the cultured mycelium *Verticillum* sp. FO-2787 [16]. Antibiotics LL-Z1272α, β, γ,

* Corresponding author. Tel.: +81 3 5841 8202; fax: +81 3 5841 3444.
E-mail address: tmogi@m.u-tokyo.ac.jp (T. Mogi).

0005-2728/$ – see front matter © 2008 Elsevier B.V. All rights reserved.
doi:10.1016/j.bbabio.2008.11.016

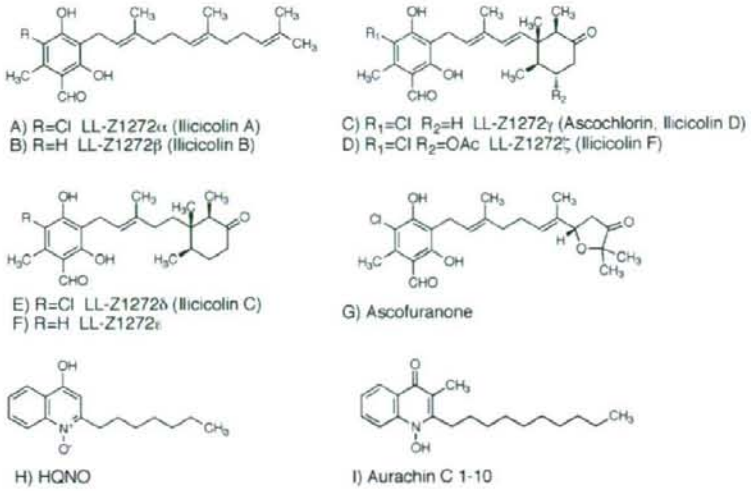

Fig. 1. Structures of antibiotics LL-Z1272 and related natural compounds.

δ, ε and ζ have been originally isolated from an imperfect fungus *Fusarium* sp. as inhibitors for the growth of the protist *Tetrahymena pyriformis* [17]. Ilicicolin A, B, D, C, and F isolated from the fungus *Cylindrocladium ilicicola* [18] are also identical to LL-Z1272α, β, γ, δ, and ζ, respectively [19]. AF and piericidin A were kind gifts from Drs. Masaichi Yamamoto (aRigen Pharmaceuticals, Inc.) and Shigeo Yoshida (Institute of Physical and Chemical Research), respectively. Synthesis of aurachin C 1-10 was described previously [20]. Antimycin A_1 and 2-heptyl-4-hydroxyquinoline *N*-oxide (HQNO) were purchased from Sigma.

2.2. Preparation of cytoplasmic membrane vesicles and purification of cytochrome bo

Cytochrome *bd*-overproduced membranes were isolated from *E. coli* ST4683/pNG2 (Δ*cyo* Δ*cyd*/*cyd*$^+$ Tet^R), which can overproduce *bd*-type quinol oxidase as the sole terminal oxidase [21]. Heme *d* content was 2.1±0.1 nmol/mg protein (*i.e.* approximately 20% of membrane proteins). Cytochrome *bo*-type quinol oxidase was purified from cytoplasmic membranes of *E. coli* GO103/pHN3795-1 (*cyo*$^+$ Δ*cyd*/*cyo*$^+$ Amp^R), as described previously [22]. Trypanosome AOX-overproduced membranes were isolated from *E. coli* FN102 (BL21 (DE3) Δ*hemA*)/pTvAOX, which can express *Trypanosoma vivax* AOX as the sole functional quinol oxidase [23]. The expression level of AOX was estimated to be ~5% of membrane proteins by SDS-polyacrylamide gel electrophoresis.

2.3. Quinol oxidase assay

The activity of the *E. coli* quinol oxidases was determined at 25 °C with a V-660 double monochromatic spectrophotometer (JASCO, Tokyo, Japan) with data acquisition at 0.05 s. The reaction mixture (1 ml) contained 50 mM potassium phosphate (pH 6.5), and 0.02% Tween 20 (protein grade, Calbiochem) [24]. Enzyme concentrations were 2.4 nM for cytochrome *bd* and 2 nM for cytochrome *bo*. Reactions were started by addition of ubiquinol-1 (Q_1H_2) at a final concentration of 100 μM, and the activity was calculated by using a molar extinction coefficient of 12,300 at 278 nm. The activity of *T. vivax* AOX was measured in 50 mM Tris–HCl (pH 7.4)–0.1% sucrose monolaurate (Mitsubishi-Kagaku Foods Co., Tokyo, Japan). Enzyme kinetics were analyzed based on the modified *ping-pong bi-bi* mechanism for cytochrome *bd* [21] or the Michaelis–Menten mechanism for cytochrome *bo* and *T. vivax* AOX, by using KaleidaGraph ver. 4.0 (Synergy Software, Reading, PA).

2.4. Dose–response analysis

Duplicate assays were performed at each concentration with two independent preparations of membranes. Dose–response data were analyzed by the nonlinear regression curve-fitting with KaleidaGraph ver. 4.0 as described previously [24]. IC_{50} values in the presence of 100 μM Q_1H_2 were estimated by using the equation for the relative residual activity; $v = 1/(1+([\text{Inhibitor}]/IC_{50})^n)$ where n is the Hill coefficient [24].

3. Results

3.1. Analysis of inhibition of cytochrome bd by antibiotics LL-Z1272

In the course of our screening for inhibitors against the *E. coli* cytochrome *bd*, we identified LL-Z1272γ as an antibiotic that suppressed the Q_1H_2 oxidation by the cytochrome *bd*-overproduced membranes (84% inhibition at 5 μg/ml) greater than antimycin A (50%), a non-competitive inhibitor of cytochrome *bd* [25]. We extended our screening with antibiotics LL-Z1272β, γ, δ, ε and ζ, prenylphenols isolated from *Verticillum* sp. FO-2787 [16], and found that LL-Z1272β and ε were more potent inhibitors for cytochrome *bd*. These compounds do not have a chlorine atom at position 5 of the phenol ring (Fig. 1), and the cyclohexanone ring of LL-Z1272ε slightly increased the binding affinity to cytochrome *bd* (Table 1). The 50% inhibitory concentrations (IC_{50}) for LL-Z1272β and ε (dechlorinated derivatives) were determined to be 2.1 and 1.1 μM (average values of two independent preparations), respectively, and are one-order of magnitude smaller than those of LL-Z1272γ, δ and ζ (chlorinated derivatives) (Table 1). The IC_{50} values for known inhibitors for cytochrome *bd* [20,25–27] are 10 μM for piericidin A, 5 μM for antimycin A, 1 μM for HQNO, and 8.3 nM for aurachin C 1–10.

Table 1
Summary on IC_{50} values of quinol oxidase inhibitors for the *E. coli* cytochrome *bd* and *bo* and *T. vivax* AOX

Compounds	Cytochrome *bd*[a]	Cytochrome *bo*[b]	trypanosome AOX[c]
LL-Z1272β	2.1±0.1[d]	1.2±0.1	0.18±0.02
LL-Z1272γ	81±17	0.082±0.016	0.015±0.001
LL-Z1272δ	32±4	0.28±0.02	0.046±0.004
LL-Z1272ε	1.1±0.1	7.2±0.7	0.65±0.09
LL-Z1272ζ	85±7	0.37±0.02	0.43±0.02
Ascofuranone	47±10	0.062±0.003	0.0049±0.0002
Aurachin C 1–10	0.0083±0.0003	0.0023±0.0001	28±2

[a] The *E. coli* cytochrome *bd*-overproduced membranes.
[b] The purified *E. coli* cytochrome *bo*.
[c] The *T. vivax* AOX-overproduced membranes.
[d] μM.

3.2. Kinetic analysis of inhibition of cytochrome bd by LL-Z1272β and ε

Effects of LL-Z1272β and ε on the Q_1H_2 oxidation by cytochrome *bd* were further analyzed kinetically. Control data were analyzed based on the modified *ping-pong bi-bi* mechanism by assuming the stabilization of dioxygen reduction intermediates [28] and apparent K_m and V_{max} values for the control were determined to 50 μM and 2364 Q_1H_2/enzyme/s, respectively, in 50 mM potassium phosphate (pH 6.5)–0.02% Tween 20 [24] (Fig. 2). In the presence of inhibitors, reactions followed the Michaelis–Menten kinetics (Fig. 2). LL-Z1272β acts as a noncompetitive inhibitor with K_i = 7.6±2.5 μM while LL-Z1272ε serves as a competitive inhibitor with K_i = 1.00±0.03 μM (Fig. 2).

3.3. Dose–response analysis of inhibition of cytochrome bo by antibiotics LL-Z1272

In contrast to *bd*-type oxidase, the Q_1H_2 oxidase activity of the *E. coli* cytochrome *bo* was more sensitive to chlorinated derivatives, LL-Z1272γ, ε and ζ. IC_{50} values for LL-Z1272β, γ, δ, ε and ζ (averages from two preparations) were determined to be 1.2, 0.082, 0.28, 7.2 and 0.37 μM, respectively (Table 1). The IC_{50} values for known inhibitors for cytochrome *bo* [20,27,29–31] are 0.3 μM for HQNO, 0.14 μM for piericidin A, and 2.3 nM for aurachin C 1–10, showing that cytochrome *bo* is more sensitive to these quinone analogs than cytochrome *bd*. It should be noted that LL-Z1272γ is a very potent inhibitor of cytochrome *bo*.

3.4. Kinetic analysis of inhibition of cytochrome bo by antibiotics LL-Z1272

Effects of LL-Z1272β, γ, δ, and ζ on the Q_1H_2 oxidation by cytochrome *bo* were further analyzed kinetically at different concentrations of inhibitors. Enzyme kinetics were analyzed based on the Michaelis–Menten mechanism [29,31], and we found that the inhibition mechanism was all mixed-type (Fig. 3). It should be noted that due to changes in assay conditions apparent K_m and V_{max} values were shifted to 23 μM and 1035 Q_1H_2/enzyme/s, respectively (Fig. 3), from 50 μM and 515 Q_1H_2/enzyme/s, respectively, in 50 mM Tris–HCl (pH 7.4)–0.1% sucrose monolaurate in our previous study [32].

3.5. Dose–response analysis of inhibition of trypanosome AOX by antibiotics LL-Z1272

Because of the structural similarity of antibiotics LL-Z1272 with trypanocidal AF (Fig. 1), we examined the effects of antibiotics LL-Z1272 on Q_1H_2 oxidase activity of *T. vivax* AOX. From dose–response analysis with the AOX-overproduced *E. coli* membranes, we determined IC_{50} values for LL-Z1272β, γ, δ, ε, ζ, AF and aurachin C1–10 to be 180, 15, 46, 650, 430, 4.9 nM and 28 μM, respectively (Table 1). Our data indicate that 1) the furanone ring of AF is not essential for binding to trypanosome AOX, 2) the 5-chloride group on the phenol ring increases the binding affinity, and 3) aurachin C, the most potent inhibitor for bacterial quinol oxidases (IC_{50} = 8.3 and 2.3 nM for the *E. coli* cytochrome *bd* and *bo*, respectively (Table 1)) [20,27], is 2 to 4 order of magnitude less active than the prenylphenols.

3.6. Kinetic analysis of inhibition of trypanosome AOX by antibiotics LL-Z1272

Effects of LL-Z1272β, γ, δ, ε and ζ and AF on enzyme kinetics by *T. vivax* AOX were examined in the presence of detergents. Q_1H_2 oxidation by *T. vivax* AOX followed the Michaelis–Menten kinetics

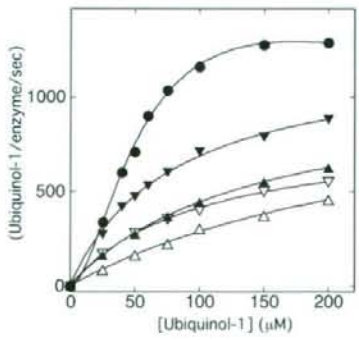

Fig. 2. Effects of antibiotics LL-Z1272 on kinetic parameters for Q_1H_2 oxidation by the *E. coli* cytochrome *bd*. Kinetic analysis was carried out in the absence of inhibitors (●) and the presence of 2 (▼) or 5 (▽) μM LL-Z1272β or 2 (▲) or 5 (△) μM LL-Z1272ε. Control data was analyzed by using the equation $v = SV_{max}/(SS(1+S/K_S)+SK_m+K_mK_m)$ where K_S indicates the constant for substrate inhibition. Data obtained in the presence of inhibitors were analyzed based on the Michaelis–Menten kinetics. The apparent K_m (μM) and V_{max} (Q_1H_2/enzyme) values obtained were 50±4 and 2364±194, respectively, for the control (K_S = 381 μM), 79±5 and 1232±33, respectively, for 2 μM LL-Z1272β, 100±5 and 826±21, respectively, for 5 μM LL-Z1272β, 140±3 and 1065±12, respectively, for 2 μM LL-Z1272ε, 287±41 and 1113±107 Q_1H_2/enzyme/s, respectively, for 5 μM LL-Z1272ε, respectively.

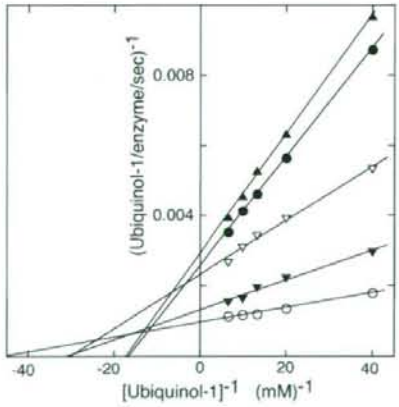

Fig. 3. Effects of antibiotics LL-Z1272 on kinetic parameters for Q_1H_2 oxidation by the *E. coli* cytochrome *bo*. Kinetic analysis was carried out in the absence of inhibitors (○) and the presence of 0.75 μM LL-Z1272β (▼), 0.2 μM LL-Z1272γ (●), 0.75 μM LL-Z1272δ (▲), and ζ (▽). Data were analyzed based on the Michaelis–Menten kinetics. The apparent K_m and V_{max} values obtained are 23±2 and 1035±28 (control), 43±4 and 841±30 (0.75 μM LL-Z1272β), 64±2 and 402±4 (0.2 μM LL-Z1272γ), 66±3 and 361±6 (0.75 μM LL-Z1272δ), 46±4 μM and 486±14 Q_1H_2/enzyme/s (0.75 μM LL-Z1272ζ), respectively. *R* values were >0.997.